Mon. Not. R. Astron. Soc. **269,** 975–997 (1994)

The spectrum of the planetary nebula NGC 6572

Siek Hyung,[1★] Lawrence H. Aller[1★] and Walter A. Feibelman[2★ †]
[1]*Astronomy Department, University of California, Los Angeles, CA 90024, USA*
[2]*Laboratory for Astronomy and Solar Physics, Code 684.1, NASA Goddard Space Flight Center, Greenbelt, MD 20771, USA*

Accepted 1994 March 18. Received 1994 March 15; in original form 1993 October 8

ABSTRACT

A detailed, high-spectral-resolution study of the spectrum of the planetary nebula NGC 6572 is made for the optical region 365 to 1005 nm, using the Hamilton echelle spectrograph of Lick Observatory, and for the ultraviolet (UV) spectral region 125 to 320 nm with the high-dispersion mode of the *International Ultraviolet Explorer* (*IUE*) satellite. NGC 6572 is a rather young planetary nebula, with a high surface brightness and a seemingly relatively regular spatial structure. This nebula and especially its central star are also variable. The rich spectrum in both the optical and UV regions offers outstanding opportunities for diagnostic studies, abundance determinations, and even checking atomic processes. The prominent line spectrum of permitted lines of C II, N II, O II etc. may arise primarily from recombination. A density-contrast model is constructed to obtain chemical abundances by two methods and to predict isophotal contours. The metal/hydrogen ratio appears to be smaller than in the Sun. We suggest that NGC 6572 originated from a star of about one solar mass, and that the core may have a mass of about 0.57 $M_{\odot}$. The expansion age of the nebula appears to be about 2600 yr.

Key words: ISM: abundances – planetary nebulae: general – planetary nebulae: individual: NGC 6572 – ultraviolet: ISM.

1 INTRODUCTION

The rich spectra of certain bright, compact planetary nebulae (PNe), such as IC 4997 and NGC 6572, provide opportunities for detailed studies of physical processes, star–nebula relationships, and establishment of bench-marks in stellar evolution studies. The spectra of both IC 4997 and NGC 6572 are to some extent variable (see Feibelman, Aller & Hyung 1992, hereafter FAH, and references therein). IC 4997 shows relatively striking changes in the nebular spectrum, while the central star seems to show small changes; the opposite appears to be true of NGC 6572. With its remarkably high density, IC 4997 stands in a class by itself, while NGC 6572 shows some close similarities to NGC 6567 (Hyung, Aller & Feibelman 1993).

Isophotic contours have been evaluated for NGC 6572 in the optical, infrared (IR), and radio-frequency (r.f.) spectral ranges. These studies indicate a fairly regular bilateral symmetry, which can be represented, at least in the first approximation, by a density-contrast model, although small regions of higher density persist.

With the VLA, Masson (1989) measured the distance of NGC 6572 as 1700 pc, a value somewhat larger than had been found by statistical methods; he emphasizes the need for a longer time baseline. Measurement of the distance is very important, for it enables us to construct nebular models etc. on an absolute scale and to speculate on evolutionary developments. Recently, a more precise distance determination of 1490 ± 220 pc was made by Hajian, Terzian & Bignell (1993, in preparation). Acker et al. (1992) have compiled an extensive bibliography for NGC 6572.

In Section 2, we describe both the optical and *IUE* observations, and tabulate line identifications and intensities on the scale $F(\mathrm{H}\beta) = 100$. We derive the coefficient of interstellar extinction, C, and give the thus corrected line intensities on the scale $I(\mathrm{H}\beta) = 100$. These data constitute the heart of this paper. In Section 3, we discuss the variability of the spectrum of the central star. Section 4 treats the nebular spectral observations with respect to both the permitted lines of He I, C II, C III, N II, N III, O I and O II, and the collisionally excited lines. Plasma diagnostics and ionic abundances are obtained from collisionally excited lines.

★E-mail (SPAN): bonnie::hyung (SH); bonnie::aller (LHA); iue::feibelman (WAF).
†Guest observer with the *IUE* satellite, which is sponsored and operated by the National Aeronautics and Space Administration, by the European Space Agency, and by the Science and Engineering Council of the UK.

Although fluorescence effects are important for O I λ8446 Å, as noted by Rudy et al. (1991), there is no clear indication that they are significant for nebular transitions of C II, C III, N II, N III and O II, except for N III lines such as $\lambda\lambda$4097 and 4103. In Section 5, we propose that the nebular spectrum of NGC 6572 can be explained by a density-contrast model, which we use to estimate nebular abundances, using also data from the literature. In our concluding remarks, we comment on the nebular evolution.

2 THE OBSERVATIONS

2.1 The UV spectrum

All of our UV data were secured with the *IUE* satellite, using the large elliptical aperture 10×23 arcsec^2. The entire optical image of the nebula falls within this aperture. Table 1(a) lists the 1991 *IUE* observations whose epoch falls between those of the 1990 and 1991 optical region measurements (see also FAH). Two low-resolution exposures, SWP 42043 (45 min) and LWP 20787 (12 min) were obtained. All fluxes were saturated in the SWP frame, but λ1911.21 C III], λ2329 O III + C II, and λ2473.9 [O II] observed on the LWP exposure were not saturated, although the background star + nebular spectrum was overexposed from 2600 to 3200 Å. The low-dispersion *IUE* data have higher accuracy than do the high-dispersion data. The old high-dispersion calibrations presented a problem for emission lines below 1500 Å in SWP and below 2300 Å in LWR/LWP, but the new calibrations corrected these problems (see Cassatella et al. 1990 and Taylor 1990, who find that the usual *IUE* accuracy for high-resolution data is ± 15 per cent for well-exposed lines). For marginal lines the errors are larger, $\sim \pm 30$ per cent. The low-resolution SWP is the only really accurate calibration so far, and the others, i.e. low-resolution LWR/LWP and both SWP and high-resolution LWR/LWP, are based ultimately on the low-resolution SWP data. In units of 10^{-13} erg cm^{-2} s^{-1}, the LWP 20787 fluxes in $\lambda\lambda$1911, 2329 and 2673 were, respectively, 619.3, 104.2 and 55.07. Table 1(b) presents the emission-line fluxes from high-dispersion SWP 42059 and LWP 20789, and also from LWP 20789. All observed fluxes in column (3) are in units of 10^{-13} erg cm^{-2} s^{-1}. The fourth column gives the adopted value of the extinction coefficient from Seaton (1979). The fifth column gives the intensities corrected to scale $I(\mathrm{H}\beta) = 100$, using the total nebular flux in Hβ, 3.83×10^{-10} erg cm^{-2} s^{-1} (Acker et al. 1992), which was measured by photoelectric photometry. It appears to be relatively stable in time. Thus fluxes relative to Hβ flux are obtainable, and may be corrected to intensities relative to Hβ intensity if the extinction parameter, C, is known. We choose $C = 0.4$, as described below. Fig. 1 shows the *IUE* spectra as observed in 1991. Some lines, notably those showing P Cygni profiles, are complicated mixtures of stellar and nebular features (see also Table 1b and, e.g., figs 8, 9 and 10 in FAH).

2.2 The optical region

All the optical-region spectroscopic measurements were secured with the Hamilton echelle spectrograph at the Shane 3-m telescope at Lick Observatory. The sky was very clear during our observations, and the seeing was good, typically less than ~ 1.5 arcsec. As usual, we secured nebular observations with a slit width of 640 μm (~ 1.2 arcsec) and a slit length of 4.0 arcsec at the centre of the PN. The nebular image rotated on the slit, and this has to be considered in the data analysis. We measured lines from 3650 to 10050 Å in 1986, 1987, 1990 and 1991, with a few supplementary observations in 1987 and 1992 in order to assess line variability. In this paper, we tabulate results for 1990 and 1991 only (see Tables 2a and 2b for the precise dates of the observations).

The echelle pattern fans out as the wavelength increases. Also, since the dispersion produced by the prism placed in the beam to separate the echelle orders decreases sharply from the violet to the red, the individual segments of the spectrum fall closer together as the long-wavelength limit is approached. Although the large CCD 2048×2048 chip could cover the whole spectrum, its efficiency is inferior to that of the TI CCD 800×800, and the spectral resolution is poor. The TI CCD 800×800 chip (dewar 8) was used in all our observations. Use of the TI CCD 800×800 pixel chip (which we found most satisfactory for our purposes) required six different chip settings, since the area of the chip was much smaller than that of the echelle pattern (see Fig. 2). Although a single setting (#121) suffices for the region shortward of 4300 Å, two settings (# #122 and 123) were employed for the region 4200 to 6000 Å, and three settings (# #124, 125 and 126) for $6000 < \lambda < 10200$ Å. Later, we replaced position #122 by #127 ($4400 < \lambda < 6897$ Å), which not only covers the most essential lines falling in this region but also allows us to tie Hα, [O III] and Hβ together on one exposure. Considerable overlap between different chip settings enables us to combine intensities more effectively.

For each of the required six positions, we must obtain measurements of the dark (to estimate read-out noise), the Th–Ar arc, the 'flat-field', and a comparison star. The IRAF deduction program was used to reduce the data. Hyung (1994) describes the reduction methods. The following is a brief account of the procedures. First, one has to eliminate read-out noise from each exposure, using the short and long dark-count exposure; then one can set the echelle aperture width for each order and trace the spectral segment. Secondly, the wavelength identification is accomplished by using the information supplied by the Th–Ar arc spectra. Finally, one can obtain the nebular absolute flux for each echelle order, by employing a response function obtained from the comparison star exposure. At this final step, the atmospheric extinction correction is made. Each echelle aperture has $\sim$5–7 pixel at FWHM (or $\sim$twice at FW near the bottom), and the centres of adjacent echelle orders are

Table 1. (a) *IUE* observations of NGC 6572 secured in 1991.

Exposure	Resolution	Date	Exposure Time
LWP20786	low	July 11	45m
LWP20787	low	July 11	12m
LWP20789	high	July 11	115m
SWP42043	low	July 11	30m
SWP42059	high	July 12/13	385m

Table 1. (b) Ultraviolet line fluxes and intensities, normalized to $I(\mathrm{H}\beta)=100$ and corrected for interstellar extinction ($C=0.40$).

$\lambda_{obs'd}$ (1)	Element (2)	F(IUE)/E-13 (3)	k_λ (4)	I(IUE) (5)	Notes (6)
1243.35	N V	24.14	1.630	7.153	{A}{1}{11}
1300.63	O I	2.35	1.487	0.611	{A}{2}
1304.85	O I	5.98	1.478	1.541	{A}{2}
1335.87	C II	5.07	1.415	1.233	{A}{2}
1372.07	O V	12.17	1.351	2.789	{A}{5}
1508.73	O V?	3.29	1.212	0.664	{A} stellar?
1548.27	C IV	7.65	1.184	1.504	{A}{5}
1550.85	C IV	7.31	1.182	1.435	{A}{5}
1550+	C IV	84.04	1.183	16.502	{A}{3}
1640.41	He II	5.46	1.136	1.027	{A}{5}
1641.05	[O I]	0.68	1.136	0.128	{A}{5}
1640+	He II	18.99	1.136	3.572	{A}{4}
1660.79	O III]	9.72	1.129	1.816	{A}{2}
1666.15	O III]	23.36	1.128	4.359	{A}{2}
1718.68	N IV	11.49	1.119	2.126	{A}{1}
1746.11	?	1.38	1.119	0.255	{A}{2}
1746.81	N III]	2.12	1.119	0.393	{A}{2}
1748.64	N III]	3.17	1.119	0.587	{A}{2}
1749.64	N III]	13.97	1.119	2.587	{A}{2}
1752.12	N III]	8.58	1.120	1.589	{A}{2}
1754.01	N III]	2.74	1.120	0.508	{A}{2}
1755.01	?	1.04	1.120	0.193	{A}{2}
1755.51	?	1.26	1.120	0.234	{A}{2}
1757.65	?	0.85	1.120	0.158	{A}{2}
1760.40	Al III	3.60	1.121	0.668	{A}{2}
1882.69	Si III]	4.86	1.195	0.965	{A}{2}
1892.04	Si III]	3.81	1.206	0.764	{A}{2}
1906.65	C III]	>66.47	1.225	>13.572	{A}{6}
1908.68	C III]	>55.54	1.228	>11.369	{A}{6}
2320.98	N III?	8.76	1.367	2.038	{B}{2}
2325.41	C II]	51.35	1.355	11.819	{B}{7}
2326.95	C II]	29.54	1.351	6.773	{B}{7}
2328.14	C II?	9.76	1.348	2.231	{B}{7}
2470.38	[O II]	53.66	1.024	9.105	{B}{2}
2723.24	?	2.31	0.709	0.293	{B}{2}
2750.14	C III?	3.78	0.686	0.470	{B}{2}
2763.81	C II?	4.60	0.675	0.566	{B}{2}
2829.16	He I	7.29	0.624	0.856	{B}{2}
2836.98	C II?	9.44	0.619	1.103	{B}{2}
2795.19	Mg II	1.50	0.650	0.180	{B}{8}
2796.17	Mg II	2.24	0.649	0.269	{B}{9}
2802.31	Mg II	2.44	0.644	0.292	{B}{10}
2803.16	Mg II	0.92	0.644	0.110	{B}{11}
2853.74	Mg I	2.48	0.607	0.287	{B}{2}
2945.13	He I	10.80	0.549	1.183	{B}{2}

Notes: {A} from high-dispersion SWP 42059P and LWP 20789; {B} from LWP 20789, 115-min high-resolution; {1} P Cyg emission component, stellar, noisy; {2} nebular emission; {3} stellar P Cyg emission component plus 2 nebular; {4} stellar P Cyg emission component + nebular He II plus [O I] nebular emission; {5} nebular emission riding on top of stellar P Cyg; {6} saturated; {7} nebular emission, split line? {8} emission component #1 of split Mg II λ2796 line; {9} emission component #2 of split Mg II λ2796 line; {10} emission component #1 of split Mg II λ2802 line; {11} emission component #2 of split Mg II λ2802 line.

Extinction-corrected $I(IUE)$ are also given, based on the scale of $I(\mathrm{H}\beta)=100$ in column (4) ($C=0.4$, see Section 2.2).

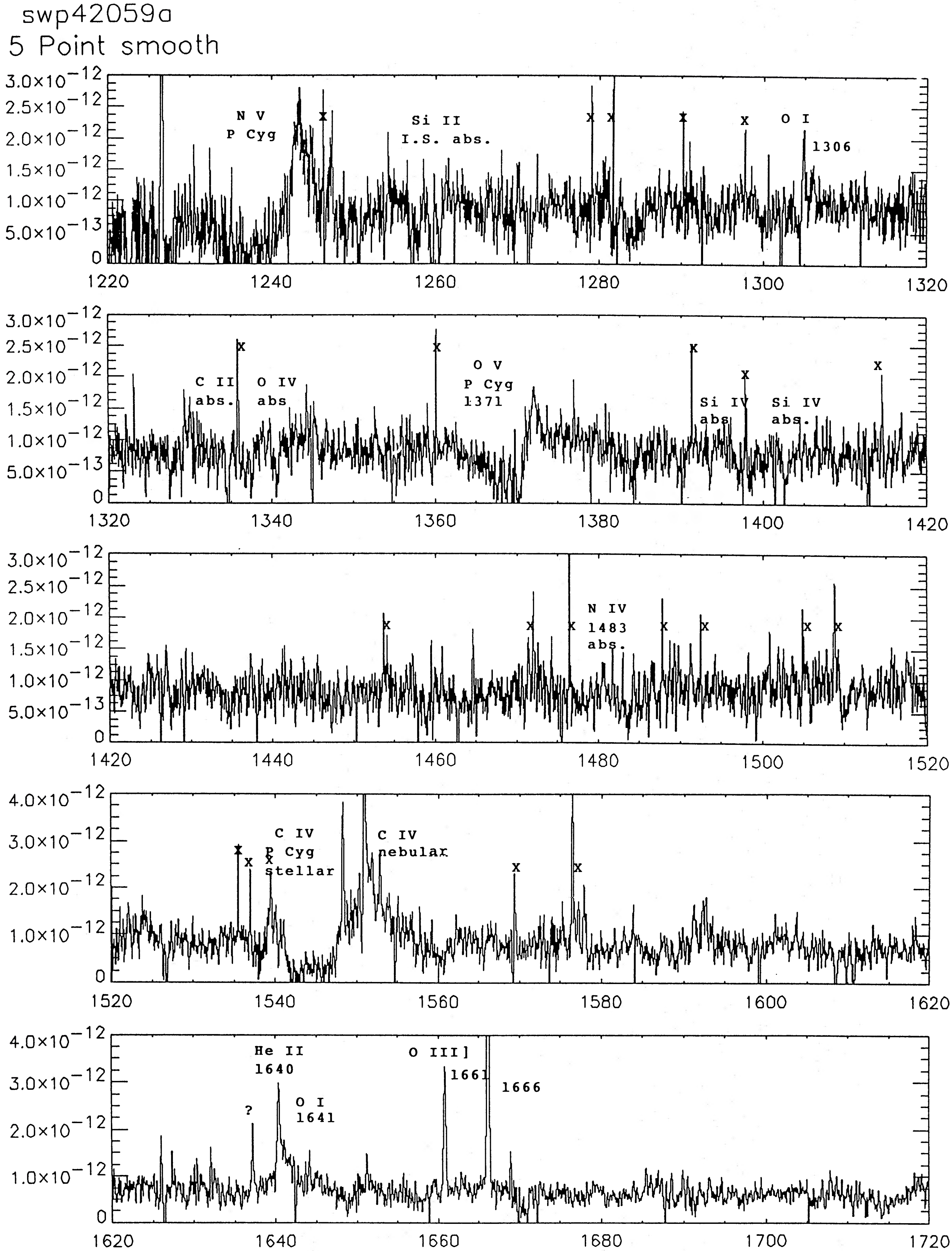

Figure 1. The ultraviolet spectrum of NGC 6572. Observations were secured with the *IUE* satellite. See text, and also FAH.

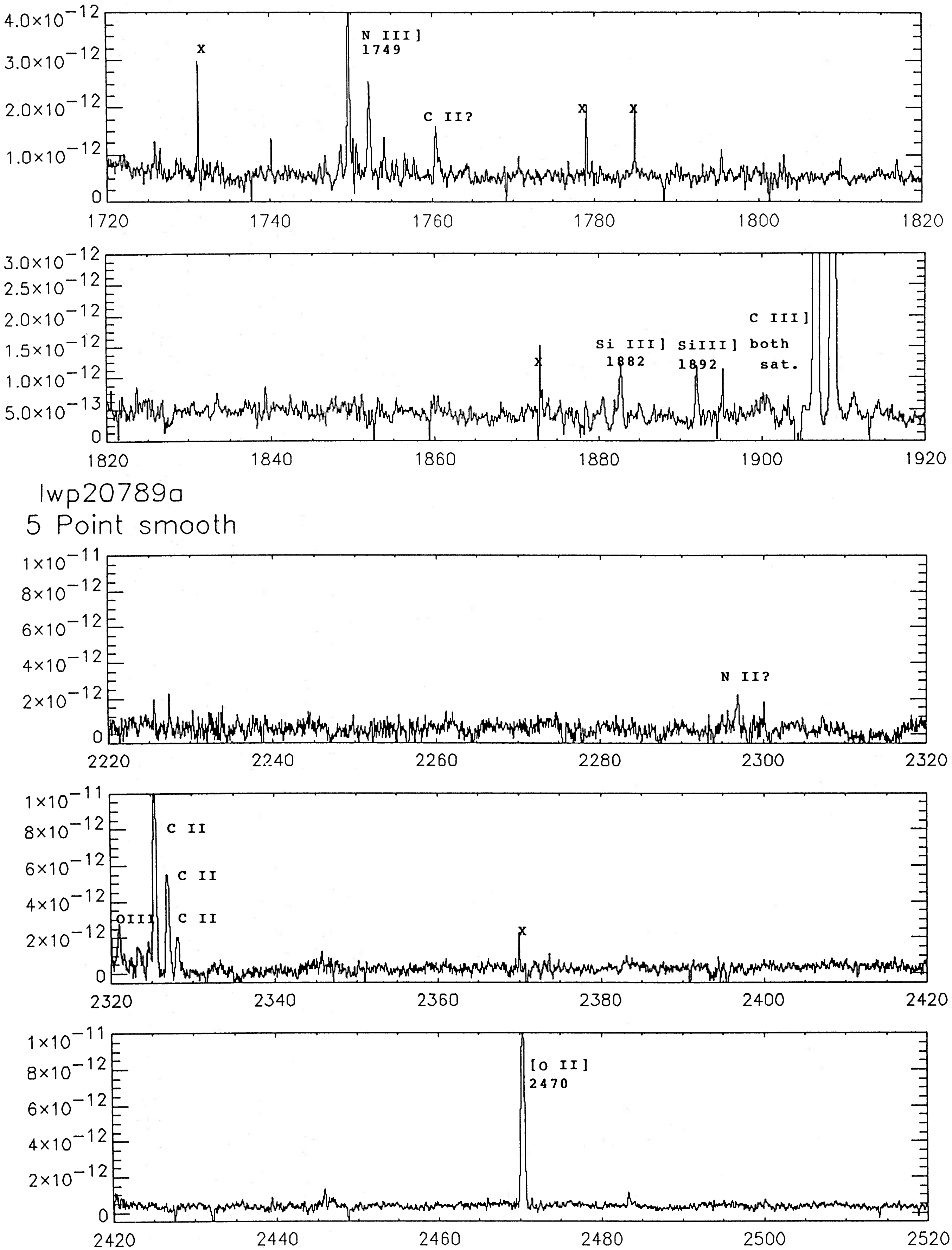

Figure 1 – *continued*

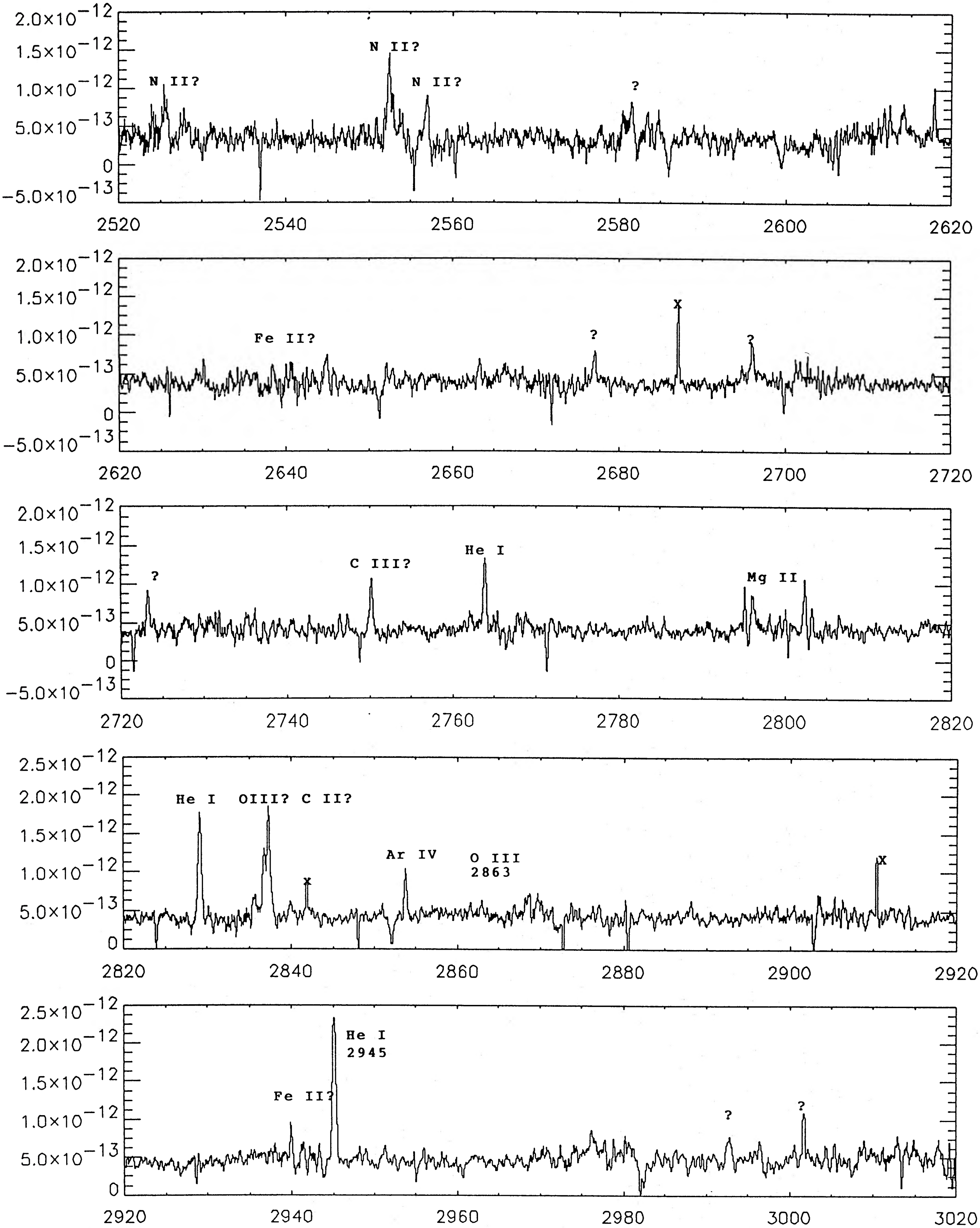

Figure 1 – *continued*

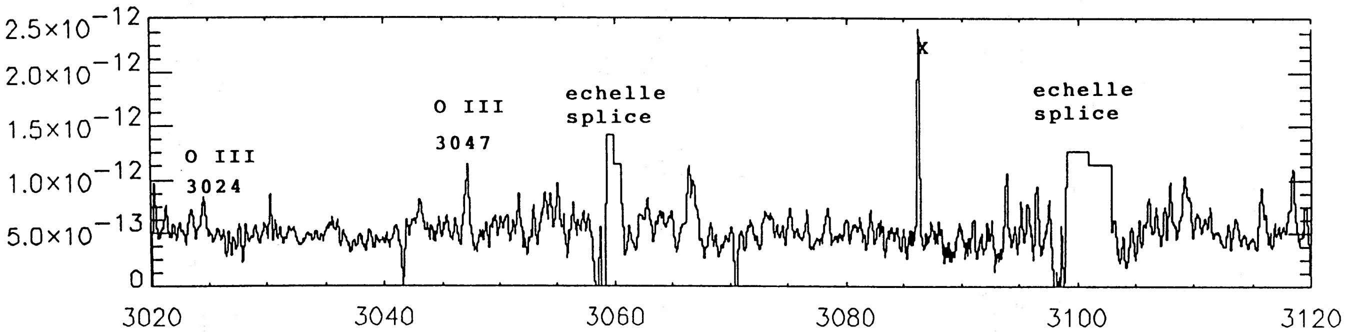

Figure 1 – *continued*

Table 2. (a) Optical observations of NGC 6572 (tabulated).

Set-up	Exp.(min)	Obs. Date(U.T.)
121	60	August 3, 1990
121	10	August 3, 1990
123	30	August 3, 1990
123	10	August 3, 1990
124	25	August 5, 1990
125	30	August 5, 1990
125	5	August 5, 1990
125	45s	August 5, 1990
126	30	August 5, 1990
126	5	August 5, 1990
127	25	August 2, 1990
127	5	August 2, 1990
127	1	August 2, 1990
127	30s	August 2, 1990
121	70	August 30, 1991
121	10	August 30, 1991
123	30	August 30, 1991
123	5	August 30, 1991
124	25	Septem. 1, 1991
125	30	August 31, 1991
125	10	August 31, 1991
125	45s	August 31, 1991
126	30	Septem. 1, 1991
126	5	Septem. 1, 1991
127	25	August 31, 1991
127	5	August 31, 1991

Table 2. (b) Optical observations of NGC 6572 (untabulated).

Set-up	Exp.(min)	Obs. Date(U.T.)
121	60	June 29, 1986
121	20	June 29, 1986
121	5	June 29, 1986
122	25	June 30, 1986
122	5	June 30, 1986
122	1	June 30, 1986
123	25	June 30, 1986
123	5	June 30, 1986
124	25	July 1, 1986
124	5	July 1, 1986
124	1	July 1, 1986
125	25	July 1, 1986
125	5	July 1, 1986
125	10s	July 1, 1986
126	25	June 30, 1986
126	5	June 30, 1986
121	30	August 4, 1987
121	5	August 4, 1987
121	5	June 18, 1992
121	1	June 18, 1992
127	25	June 18, 1992
127	30s	June 18, 1992

well separated, by 15–23 pixel. For a number of differently adopted aperture widths for each echelle order, i.e. whether the widths are adopted at FWHM or at near the bottom, we do not find any noticeable difference in the final absolute flux calibration or any difficulty in estimating the background: the error from this cause seems to be negligible, maybe less than ~ 1 per cent for most echelle orders.

Table 3 summarizes the results obtained for 1990 and 1991. Column (1) gives the observed wavelength corrected for the relative radial velocity of nebula and observer, column (2) the laboratory wavelength for the line identified in column (3). Column (4) gives the multiplet number from Moore's Revised Multiplet Table. The extinction coefficient, k_λ, as defined by Seaton (1979), is given in column (5). Then columns (6) and (8) give the observed line fluxes on the scale $F(\mathrm{H}\beta)=100$. Likewise columns (7) and (9) give the line intensities on the scale $I(\mathrm{H}\beta)=100$, on the assumption that the extinction parameter $C=\log[I(\mathrm{H}\beta)/F(\mathrm{H}\beta)]=0.4$, where $I(\mathrm{H}\beta)$ and $F(\mathrm{H}\beta)$ are, respectively, the corrected Hβ intensity and the observed Hβ flux, both given in absolute units.

In the present instance, we used mainly the Balmer decrement, Paschen and Balmer lines of the same upper

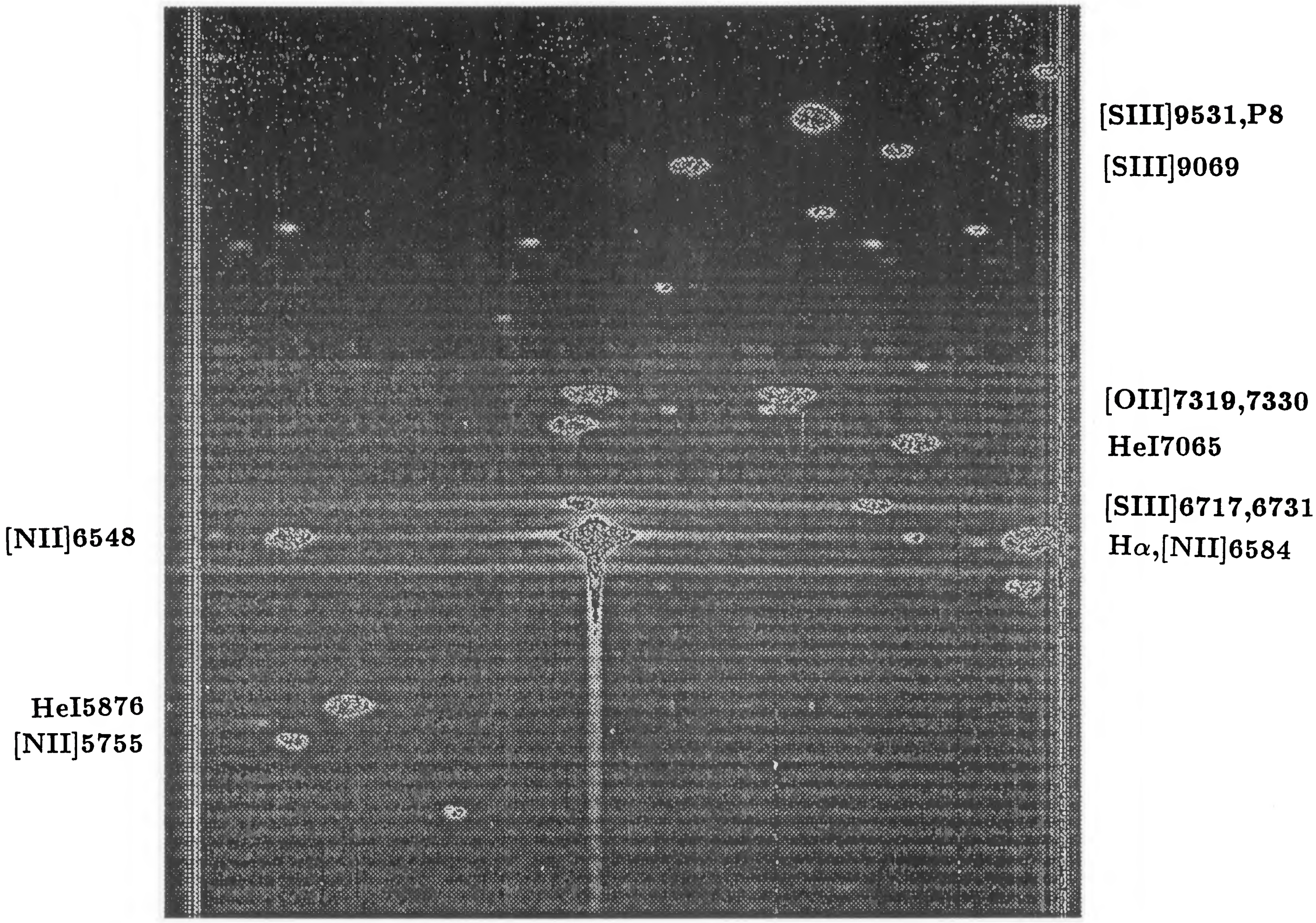

Figure 2. Hamilton echelle spectra of the Hα region (1993 August 31, 5-min dwell time). The heavily overexposed Hα image 'drips' downward through adjacent orders.

quantum number, n, and a comparison of Hβ and r.f. fluxes. The Balmer decrement gave 0.49 ± 0.03, the Paschen/Balmer ratio gave 0.44 ± 0.02, while, from a comparison of Hβ and 5-GHz fluxes, Milne & Aller (1975) found 0.31. We adopted $C = 0.4$.

Several procedures are available for estimating the accuracy of the measurements. By comparing data obtained on different nights and with different chip settings, we can assess the effect of guiding errors, and the influence (if any) of position in field, and of response function. Errors arising from these effects were of the order of 3–6 per cent, and were random in character. Another estimate is provided by measurements of lines arising from the same upper level, whose A-values are accurately known. Finally, there is the consistency check provided by the Balmer decrement after interstellar extinction is evaluated. On our scale, $I(\mathrm{H}\beta) = 100$, lines weaker than 0.05 have errors of 30–60 per cent; for lines in the range $0.05 \le I \le 0.10$, errors fall in the interval 25–40 per cent; for $0.10 \le I \le 0.30$, errors of 15–30 per cent are expected; for $0.3 \le I \le 1.0$, typical errors are 10–25 per cent; and for stronger lines, we estimate errors of 5–10 per cent. The errors increase towards the ends of each order and, of course, with an increase in the underlying noise. Lines affected by 'bleeding' from a strong line in a nearby order may be seriously impacted. By taking a graded series of exposures, this difficulty can often be overcome.

In the optical and UV spectral regions we find nebular lines of the following ions: H, He I, C I, C II, C III, C IV, N I, [N I], N II, [N II], N III, O I, [O I], O II, [O II], [O III], Ne II, [Ne II], Mg I, Mg II, Si II, Si III, Si IV, [S II], [S III], [Cl II], [Cl III], [Cl IV], [Ar III], [Ar IV], [K IV], [Fe II], [Fe III] and [Fe IV]. The general excitation level of NGC 6572 is moderate (excitation class 5). High-excitation lines, such as N V and C IV $\lambda\lambda$5801, 5812, show diffuse, Wolf–Rayet-type profiles, and are clearly of stellar origin.

The near-IR shows a number of interesting lines (Rudy et al. 1991), e.g., [P II] 11468, 11883 Å from whose intensities they estimate a phosphorus abundance of log $N(\mathrm{P}) = 5.56$ on the scale log $N(\mathrm{H}) = 12$. Farther in the infrared are observed 12.8 μm [Ne II], 9.0 μm [Ar III] (a 'coronal'-type transition), and 10.5 μm [Si IV] (see, e.g., Beck et al. 1981). We use these data (see Tables 9 and 10) in a determination of nebular abundances. There are a number of important far-IR transitions that will require measurements made from space or with the Kuiper Airborne Observatory. A discussion of these possibilities lies outside the scope of this paper.

3 THE SPECTRUM OF THE CENTRAL STAR OF NGC 6572

The central star may well have had a long history of spectral variability. From his observations in 1916, Wright (1918)

Table 3. Spectrum of NGC 6572.

$\lambda_{obs'd}$ (1)	λ_{lab} (2)	Element (3)	Mult. (4)	k_λ (5)	$F(1990)$ (6)	$I(1990)$ (7)	$F(1991)$ (8)	$I(1991)$ (9)
3657.20	3657.27	H I	H36	0.276	0.03	0.036	0.02	0.032
3657.91	3657.93	H I	H35	0.275	0.05	0.065	0.04	0.056
3658.65	3658.64	H I	H34	0.275	0.07	0.092	0.06	0.071
3659.42	3659.42	H I	H33	0.275	0.10	0.126	0.09	0.111
3660.27	3660.28	H I	H32	0.275	0.14	0.177	0.12	0.151
3661.23	3661.22	H I	H31	0.275	0.17	0.225	0.17	0.214
3662.25	3662.26	H I	H30	0.274	0.17	0.224	0.20	0.252
3663.42	3663.41	H I	H29	0.274	0.17	0.219	0.21	0.265
3664.66	3664.68	H I	H28	0.274	0.22	0.278	0.24	0.314
3666.08	3666.10	H I	H27	0.273	0.19	0.250	0.30	0.381
3667.69	3667.88	H I	H26	0.273	0.27	0.348	0.29	0.367
3669.48	3669.47	H I	H25	0.272	0.29	0.377	0.33	0.419
3670.82				0.272	0.07	0.084	0.77	0.984
3671.45	3671.48	H I	H24	0.272	0.35	0.443	0.45	0.579
3673.76	3673.76	H I	H23	0.271	0.36	0.462	0.34	0.441
3676.38	3676.36	H I	H22	0.270	0.41	0.532	0.47	0.597
3679.35	3679.35	H I	H21	0.270	0.43	0.548	0.47	0.600
3682.80	3682.81	H I	H20	0.269	0.52	0.666	0.56	0.717
3686.83	3686.83	H I	H19	0.268	0.64	0.813	0.65	0.838
3691.55	3691.56	H I	H18	0.267	0.76	0.967	0.75	0.963
3694.23	3694.22	Ne II	(1)	0.266	0.07	0.088	0.05	0.063
3697.16	3697.15	H I	H17	0.265	0.82	1.045	0.83	1.062
3702.73	3702.90	O III	(14)	0.264	0.14	0.179	0.17	0.216
3703.88	3703.86	H I	H16	0.272	1.12	1.444	0.84	1.081
3705.00	3705.02	He I	(25)	0.271	0.57	0.737	0.54	0.693
3707.27	3707.24	O III	(14)	0.271	0.19	0.244	0.20	0.253
3709.83	3709.64	Ne II	(1)	0.270	0.05	0.059	0.10	0.123
	3709.52	O III	(21)					
3711.96	3711.97	H I	H15	0.269	1.12	1.438	1.10	1.412
3713.08	3712.75	O II	(3)	0.269	0.05	0.066	0.07	0.095
3714.02	3714.03	N III	(14)	0.269	0.11	0.139	0.10	0.123
3715.09	3715.08	O III?	(14)	0.269	0.15	0.197	0.13	0.160
3721.90	3721.94	H I	H14	0.267	1.84	2.353	1.67	2.132
	3721.83	[S III]	(2F)					
3726.01	3726.03	[O II]	(1F)	.266	13.21	16.875	10.38	13.251
3727.31	3727.33	O II	(3)	0.265	0.03	0.037	0.04	0.046
3728.76	3728.82	[O II]	(1F)	0.265	5.11	6.515	4.15	5.296
3732.89	3732.99	He I	(24)	0.264	0.05	0.062	0.04	0.051
3734.36	3734.37	H I	H13	0.263	1.73	2.200	1.70	2.164
3737.66				0.262	0.03	0.037	0.05	0.063
3750.14	3750.15	H I	H12	0.259	2.08	2.646	2.11	2.677
3754.68	3754.67	O III	(2)	0.258	0.18	0.227	0.21	0.269
3756.06	3756.10	He I	(66)	0.257	0.04	0.057	0.03	0.036
	3757.60	N III	(11)					
3757.28	3757.21	O III	(2)	0.257	0.07	0.094	0.08	0.098
3759.88	3759.81	O III+?	(2)+?	0.256	0.19	0.235	0.25	0.320
3762.29	3762.63	OII,NIII	(31)(11)	0.256	0.03	0.034	0.02	0.030
3770.53	3770.63	H I	H11	0.254	3.01	3.806	2.82	3.560
3774.04	3774.00	O III?	(2)	0.253	0.06	0.070	0.07	0.090
3777.11	3777.16	Ne II	(1)	0.252	0.03	0.034	0.02	0.023
3784.97	3785.01	O II	(95)	0.250	0.06	0.069	0.04	0.056
	3784.89	He I	(64)					
3791.33	3791.26	O III?	(2)	0.248	0.06	0.069	0.05	0.065
3797.91	3797.90	H I	H10	0.246	3.70	4.640	3.73	4.683
3805.77	3805.77	He I	(63)	0.244	0.05	0.068	0.07	0.082
3809.14				0.243	0.02	0.028	0.03	0.038
3819.61	3819.61	He I	(22)	0.241	1.00	1.245	0.97	1.206
3831.64				0.237	0.04	0.045	0.04	0.052
3833.55	3833.57	He I	(62)	0.237	0.07	0.082	0.06	0.070
3835.38	3835.39	H I	H9	0.236	5.62	6.992	5.38	6.693
3838.27	3838.09	He I	(61)	0.236	0.03	0.033	0.04	0.051
3842.83				0.235	0.12	0.146	0.04	0.047
	3856.16	O II	(12)					
3856.04	3856.02	Si II	(1)	0.231	0.05	0.058	0.04	0.051
3862.56	3862.59	Si II	(1)	0.229	0.09	0.108	0.13	0.157
	3864.13	O II	(11)					
3864.46	3864.45	O II	(12)	0.229	0.05	0.060	0.01	0.011
3867.55	3867.63	He I	(20)	0.228	0.28	0.341	0.05	0.065
3868.75	3868.71	[Ne III]	(1F)	0.228	77.27	95.317	71.12	87.733
3871.83	3871.82	He I	(60)	0.227	0.12	0.152	0.10	0.123
3875.08				0.226	0.03	0.031	0.04	0.048
3878.13				0.226	0.01	0.017	0.02	0.029
3882.33	3882.20	O II	(12)	0.224	0.03	0.035	0.03	0.033
3888.95	3889.05	H I	H8	0.223	13.21	16.223	12.30	15.105
	3888.65	He I	(2)					
3918.93	3919.29	O II	(17)	0.215	0.03	0.036	0.02	0.027
	3918.99	C II	(9)					
3920.65	3920.68	C II	(4)	0.215	0.03	0.037	0.04	0.044
3933.74		Ca II	ISM	0.212	0.212Å	abs	0.203Å	abs
3964.73	3964.73	He I	(5)	0.204	0.88	1.058	0.87	1.051

Table 3 – *continued*

$\lambda_{obs'd}$ (1)	λ_{lab} (2)	Element (3)	Mult. (4)	k_λ (5)	F(1990) (6)	I(1990) (7)	F(1991) (8)	I(1991) (9)
3967.46	3967.41	[Ne III]	(1F)	0.203	25.18	30.366	23.71	28.601
3970.07	3970.07	H I	Hϵ	0.203	14.00	16.871	13.12	15.817
3973.21	3973.26	O II	(6)	0.202	0.03	0.031	0.02	0.020
3974.05	3973.84	C II	(37)	0.202	0.02	0.021	0.02	0.020
	4024.04	O II	(99)					
4023.96	4023.99	He I	(54)	0.190	0.02	0.024	0.04	0.046
4026.20	4026.36	He I	(18)	0.189	2.15	2.557	2.10	2.499
4027.28				0.189	0.03	0.034	0.03	0.038
4041.33	4041.32	N II?	(39)	0.186	0.02	0.022	0.03	0.039
	4041.31	O II	(50)					
4043.63	4043.53	N II	(39)	0.185	0.05	0.055	0.02	0.024
4046.43				0.185	0.02	0.021	0.02	0.022
4060.84	4060.98	O II	(97)	0.181	0.02	0.020	0.03	0.030
4068.57	4068.60	[S II]	(1F)	0.180	1.14	1.339	0.97	1.150
4069.93	4069.90	O II	(10)	0.179	0.14	0.171	0.17	0.204
	4069.64	O II	(10)					
4072.23	4072.16	O II	(10)	0.179	0.12	0.143	0.16	0.185
4074.16	4073.90	O III	(23)	0.178	0.03	0.034	0.04	0.050
4076.19	4076.35	[S II]	(1F)	0.178	0.50	0.592	0.45	0.525
4078.85	4078.86	O II	(10)	0.177	0.02	0.021	0.02	0.028
4081.03	4081.10	O II?	(23)	0.177	0.02	0.021	0.02	0.029
4083.88	4083.90	O II	(49)	0.176	0.01	0.018	0.02	0.027
	4085.25	O II	(10)					
4085.08	4084.66	O II	(21)	0.176	0.02	0.029	0.03	0.033
4087.14	4087.16	O II	(48)	0.175	0.02	0.025	0.02	0.020
	4089.30	O II neb	(48)					
4089.25	4089.25	Si IV^{WR}	(1)	0.175	0.516Å	em	0.473Å	em
	4088.86	O II	(1)					
4092.92	4092.94	O II	(10)	0.174	0.03	0.035	0.03	0.034
4097.35	4097.31	N III	(1)	0.173	0.69	0.813	0.73	0.856
	4097.27	O II	(20;48)					
4101.75	4101.76	H I	Hδ	0.172	26.36	30.890	23.82	27.914
4103.40	4103.37	N III	(1)	0.172	0.41	0.483	0.47	0.552
4104.94	4105.00	O II	(20)	0.171	0.06	0.068	0.08	0.097
4107.13	4107.07	O II	(47)	0.171	0.03	0.035	0.04	0.048
4108.77				0.170	0.01	0.013	0.03	0.041
4110.77	4110.80	O II	(20)	0.170	0.02	0.026	0.03	0.033
4116.10	4116.10	Si IV	(1)	0.169	0.02	0.018	0.02	0.021
4119.22	4119.22	O II	(20)	0.168	0.05	0.058	0.06	0.068
4120.81	4120.81	He I	(16)	0.168	0.26	0.309	0.30	0.355
4128.70	4128.65	Ar II?		0.166	0.02	0.022	0.03	0.035
4131.59	4131.50		WR	0.165	0.361Å	em	0.338Å	em
4132.81	4132.80	O II	(19)	0.165	0.02	0.027	0.03	0.038
	4143.77	O II	(106)					
4143.75	4143.76	He I	(53)	0.163	0.33	0.389	0.33	0.385
4146.04	4146.00	O II	(106)	0.162	0.03	0.031	0.03	0.030
	4156.54	O II	(19)					
4156.40	4156.50	C III	(21)	0.160	0.02	0.027	0.03	0.030
4162.73	4163.25	[K V]?	(1F)	0.158	0.02	0.019	0.04	0.043
4169.05	4168.97	He I	(52)	0.157	0.06	0.074	0.05	0.063
	4169.23	O II	(19)					
4186.95	4187.05	C III	(18)	0.154	0.05	0.053	0.05	0.060
4189.77	4189.79	O II	(36)	0.154	0.04	0.048	0.05	0.056
4195.72	4195.70	N III	(6)	0.153	0.02	0.023	0.02	0.018
4200.00	4199.83	He II	(3)	0.152	0.09	0.105	0.04	0.050
4219.80	4219.76	Ne II?	(52)	0.149	0.02	0.020	0.02	0.024
4241.82	4241.79	N II	(47;48)	0.145	0.02	0.023	0.03	0.029
4253.98	4253.86	O II	(10)	0.143	0.03	0.031	0.03	0.030
4267.15	4267.18	C II	(6)	0.141	0.40	0.451	0.43	0.488
4283.35	4283.13	O II	(67)	0.138	0.03	0.033	0.02	0.020
4285.66	4285.70	O II	(78)	0.138	0.02	0.021	0.02	0.019
4292.31	4292.23	O II	(78)	0.137	0.02	0.017	0.02	0.021
4294.83	4294.82	O II	(54)	0.136	0.02	0.022	0.03	0.029
4303.85	4303.82	O II	(54)	0.135	0.04	0.043	0.03	0.029
4317.18	4317.14	O II	(2)	0.133	0.04	0.051	0.05	0.053
4319.64	4319.69	O II	(2)	0.132	0.04	0.041	0.03	0.037
4325.89	4325.76	O II+?	(2)	0.131	0.03	0.030	0.04	0.047
4332.55	4332.76	O II	(65)	0.130	0.04	0.040	0.03	0.031
4336.83	4336.86	O II	(2)	0.129	0.03	0.037	0.02	0.021
4340.45	4340.47	H I	Hγ	0.129	42.17	47.485	39.99	45.035
4345.42	4345.56	O II	(2)	0.128	0.06	0.067	0.06	0.071
4347.35	4347.20	S II	(16)	0.128	0.01	0.013	0.01	0.013
4348.26	4348.36	N III	(10)	0.128	0.01	0.009	0.03	0.028
4349.24	4349.42	O II	(2)	0.127	0.08	0.093	0.07	0.077
4351.27	4351.27	O II	(16)	0.127	0.02	0.017	0.02	0.023
4353.58	4353.60	O II	(76)	0.126	0.01	0.013	0.01	0.012
4363.18	4363.21	[O III]	(2F)	0.124	7.41	8.306	7.94	8.900
4366.88	4366.90	O II	(2)	0.123	0.04	0.046	0.06	0.073
	4368.30	O I	(51)					
4368.19	4368.14	C II?	(45)	0.122	0.03	0.038	0.03	0.037

Table 3 – *continued*

$\lambda_{obs'd}$ (1)	λ_{lab} (2)	Element (3)	Mult. (4)	k_λ (5)	F(1990) (6)	I(1990) (7)	F(1991) (8)	I(1991) (9)
4379.01	4379.09	N III	(17)	0.119	0.05	0.059	0.08	0.090
4387.93	4387.93	He I	(51)	0.117	0.60	0.671	0.59	0.656
4390.51	4390.59	Mg II?	(10)	0.116	0.01	0.008		
4391.98	4391.94	Ne II?	(57)	0.116	0.02	0.023	0.02	0.023
4414.92	4414.91	O II	(5)	0.110	0.03	0.037	0.03	0.038
4416.98	4416.98	O II	(5)	0.109	0.04	0.041	0.04	0.044
4428.41	4428.54	Ne II?	(56;61)	0.106	0.02	0.018	0.02	0.020
4430.83	4430.90	Ne II?	(56)	0.106	0.01	0.014	0.03	0.036
4432.62	4432.74	N II	(55)	0.105	0.01	0.012	0.01	0.008
4437.55	4437.55	He I	(50)	0.104	0.08	0.093	0.10	0.105
4448.65	4448.21	O II(?)	(35)	0.101	0.02	0.017	0.02	0.018
4452.32	4452.38	O II	(5)	0.100	0.01	0.012	0.01	0.009
4465.42	4465.40	O II	(94)	0.096	0.03	0.029	0.04	0.040
4466.31	4466.32	O II	(87)	0.096	0.01	0.010	0.01	0.008
4467.84	4467.88	O II	(94)	0.096	0.02	0.023	0.02	0.024
4469.37	4469.32	O II	(59;94)	0.095	0.02	0.018	0.02	0.018
4471.51	4471.50	He I	(14)	0.095	4.85	5.296	5.14	5.610
	4481.33	Mg II	(4)					
4481.21	4481.13	Mg II	(4)	0.092	0.03	0.035	0.03	0.032
4488.13	4488.15	N II	(21)	0.091	0.01	0.013	0.03	0.031
	4488.09	O II	(104)					
4491.31	4491.25	O II	(86)	0.090	0.02	0.024	0.03	0.029
	4510.93	[K IV]?						
4510.90	4510.92	N III	(3)	0.085	0.04	0.047	0.05	0.056
4518.14	4518.18	N III	(3)	0.083	0.02	0.021	0.02	0.022
4523.60	4523.60	N III	(3)	0.082	0.02	0.020	0.02	0.019
4529.62	4529.70	O III?	(32)	0.080	0.01	0.011	0.01	0.010
4530.55	4530.84	N III	(3)	0.080	0.01	0.013	0.02	0.017
4533.50				0.079	0.01	0.011	0.02	0.023
4534.57	4534.57	N III	(3)	0.079	0.02	0.021	0.03	0.028
4539.65				0.078	0.02	0.020	0.01	0.011
4541.62	4541.59	He II		0.077	0.01	0.010	0.04	0.045
4543.52	4543.50		WR	0.077	0.656Å	em	0.574Å	em
4544.85	4544.80	N III?	(12)	0.076	0.05	0.058	0.02	0.020
4562.53	4562.05	Ne II?	(64)	0.072	0.03	0.028	0.03	0.031
4571.10	4571.00	Mg I	(1)	0.070	0.29	0.309	0.30	0.324
4590.88	4590.97	O II	(15)	0.065	0.04	0.045	0.04	0.046
4596.17	4596.17	O II	(15)	0.064	0.04	0.037	0.05	0.054
4604.93	4604.90		WR	0.061	0.810Å	em	0.598Å	em
4607.02	4607.13	[Fe III];N II	(3F)(5)	0.061	0.02	0.018	0.03	0.033
4609.43	4609.42	O II	(93)	0.060	0.03	0.030	0.03	0.034
4610.38	4610.14	O II	(92)	0.060	0.02	0.019	0.03	0.030
4613.76	4613.80		WR	0.059	0.123Å	em	0.086Å	em
	4613.67	O II	(92)					
4619.94				0.058	0.12	0.121	0.15	0.154
4630.40	4630.54	N II	(5)	0.055	0.03	0.027	0.03	0.028
4634.17	4634.16	N III	(2)	0.054	0.33	0.342	0.33	0.343
4638.86	4638.85	O II	(1)	0.053	0.07	0.071	0.07	0.074
4639.92	4640.64	N III	WR	0.053	0.613Å	em	0.599Å	em
4640.64	4640.64	N III	(2)	0.053	0.63	0.661	0.64	0.672
4641.85	4641.90	N III	(2)	0.052	0.20	0.209	0.25	0.259
	4641.81	O II	(1)					
4647.42	4647.40	C III	(1)	0.051	0.09	0.090	0.11	0.117
4649.13	4649.14	O II	(1)	0.051	0.22	0.234	0.27	0.280
	4650.84	O II	(1)					
4650.36	4650.16	C III	(1)	0.050	0.09	0.096	0.10	0.106
	4651.35	C III	(1)					
4651.08	4650.84	O II	(1)	0.050	0.04	0.043	0.03	0.035
4657.06	4658.64	CIV	WR	0.049	0.401Å	em	0.380Å	em
4657.77	4658.10	[Fe III]	(3F)	0.049	0.04	0.041	0.06	0.064
4658.41	4658.64	C IV	(8)	0.049	0.04	0.045	0.03	0.028
4661.67	4661.64	O II	(1)	0.048	0.07	0.077	0.09	0.098
4669.34	4669.53	O II?	(89)	0.046	0.01	0.010	0.01	0.013
4673.76	4673.75	O II	(1)	0.045	0.01	0.006	0.01	0.014
4676.23	4676.23	O II	(1)	0.044	0.05	0.056	0.06	0.058
4684.47	4685.68	He II 4686	WR	0.042	10.54Å	em	9.894Å	em
4685.77	4685.68	He II		0.042	0.37	0.384	0.37	0.389
4699.15	4699.21	O II	(25)	0.039	0.02	0.023	0.02	0.019
	4701.62	[Fe III]	(3F)					
4701.31	4701.23	O II	(58)	0.038	0.05	0.052	0.04	0.042
4705.29	4705.36	O II	(25)	0.038	0.02	0.018	0.03	0.030
4711.39	4711.34	[Ar IV]	(1F)	0.036	0.86	0.894	0.88	0.909
4713.18	4713.14	He I	(12)	0.036	0.75	0.777	0.70	0.723
4740.23	4740.20	[Ar IV]	(1F)	0.029	2.20	2.258	2.42	2.482
4769.27	4769.60	[Fe III]	(3F)	0.023	0.02	0.024	0.03	0.029
4851.35	4851.10	Mg II	(25)	0.002	0.05	0.046	0.02	0.023
4861.33	4861.33	H I	Hβ	0.000	100.00	100.000	100.00	100.000
4871.40	4871.58	O II	(57)	-0.002	0.05	0.047	0.07	0.074
4906.22	4906.70	[Fe IV]	(2F)	-0.011	0.03	0.032	0.04	0.036
4921.94	4921.93	He I	(48)	-0.015	1.35	1.334	1.55	1.532

Table 3 – *continued*

$\lambda_{obs'd}$ (1)	λ_{lab} (2)	Element (3)	Mult. (4)	k_λ (5)	F(1990) (6)	I(1990) (7)	F(1991) (8)	I(1991) (9)
4924.44	4924.60	O II	(28)	-0.015	0.05	0.049	0.07	0.065
4931.22	4931.30	[O III]	(1F)	-0.017	0.11	0.109	0.18	0.174
4948.62	4947.38	[Fe II]?	(20F)	-0.021	0.10	0.102	0.18	0.176
4956.12				-0.023	0.08	0.080	0.08	0.082
4958.94	4958.92	[O III]	(1F)	-0.023	380.19	372.166	371.54	363.694
4969.35	4969.00	[Fe VI]		-0.026	0.10	0.101	0.20	0.192
4985.57	4985.50	[Fe III]?		-0.029	0.02	0.019	0.01	0.013
4996.26		in IC 4997		-0.032	0.40	0.386	0.34	0.329
5006.86	5006.84	[O III]	(1F)	-0.034	1142.88	1107.544	1111.73	1077.360
5015.68	5015.68	He I	(4)	-0.036	2.31	2.232	2.95	2.855
5017.47	5017.63	Ar II?	(13)	-0.036	0.24	0.230	0.66	0.642
5022.78				-0.038	0.02	0.016	0.04	0.036
5029.39				-0.039	0.01	0.012	0.08	0.076
5031.96	5032.40	[Fe IV]	(1)	-0.040	0.03	0.034	0.05	0.049
5035.80	5035.77	[Fe II]?		-0.040	0.02	0.018	0.03	0.031
5041.09	5041.06	Si II	(5)	-0.041	0.07	0.070	0.08	0.075
5047.77	5047.74	He I	(47)	-0.043	0.19	0.179	0.19	0.185
5056.30	5056.35	.02 Si II	(5)	-0.045	0.08	0.073	0.11	0.105
5058.66				-0.045	0.14	0.137	0.19	0.184
5121.84	5121.69	C II	(12)	-0.058	0.02	0.016	0.01	0.013
5131.03				-0.060	0.02	0.020	0.02	0.020
	5146.06	O I?	(28)					
5145.79	5145.80	[Fe VI]		-0.063	0.02	0.019	0.02	0.019
5191.68	5191.80	[Ar III]	(3F)	-0.073	0.10	0.097	0.12	0.111
5197.90	5197.90	[N I]	(1F)	-0.074	0.12	0.113	0.15	0.138
5200.28	5200.26	[N I]	(1F)	-0.074	0.08	0.072	0.10	0.093
5270.38	5270.40	[Fe III]	(1F)	-0.089	0.04	0.039	0.03	0.031
5342.38				-0.104			0.02	0.022
5346.02	5345.67	S II?	(38)	-0.105	0.06	0.058	0.06	0.057
5411.72	5411.52	He II	WR	-0.118	0.510Å	em	0.370Å	em
5460.58				-0.128	0.02	0.020	0.03	0.030
5512.80	5512.71	O I	(25)	-0.138	0.02	0.014	0.02	0.014
5517.66	5517.71	[Cl III]	(1F)	-0.139	0.18	0.158	0.19	0.170
5518.75	5519.30	[Ni IV]?+?		-0.140	0.02	0.019	0.02	0.018
5535.37	5535.39	N II	(63)	-0.143	0.01	0.012	0.01	0.013
5537.85	5537.88	[Cl III]	(1F)	-0.143	0.43	0.375	0.45	0.397
5555.14	5554.94	O I	(24)	-0.147	0.01	0.012	0.01	0.009
5571.83	5571.83		WR	-0.150	0.395Å	em	0.432Å	em
5577.40	5577.34	[O I]	(3F)	-0.152	0.08	0.067	0.07	0.061
5592.25	5592.37	O III	(5)	-0.155	0.01	0.011	0.01	0.007
5666.60	5666.64	N II	(3)	-0.172	0.03	0.029	0.03	0.023
5676.04	5676.02	N II	(3)	-0.174	0.02	0.013	0.02	0.019
5679.65	5679.56	N II	(3)	-0.175	0.25	0.216	0.06	0.052
5754.69	5754.64	[N II]	(3F)	-0.191	1.74	1.458	2.04	1.713
5801.04	5801.51	C IV^{WR}	(1)	-0.201	2.63Å	em	1.90Å	em
5811.86	5812.14	C IV^{WR}	(1)	-0.203	1.09Å	em	1.2Å	em
5861.02				-0.213	0.01	0.009	0.01	0.006
5867.74	5867.80	He II+?		-0.214	0.10	0.078	0.10	0.079
5875.67	5875.67	He I	(11)	-0.216	20.65	16.927	19.72	16.166
5890.06	5890.05	Na I	ISM	-0.219	0.098Å	abs	0.099Å	abs
5896.08	5896.05	Na I	ISM	-0.220	0.041Å	abs	0.041Å	abs
5958.68	5958.58	O I	(23)	-0.230	0.02	0.014	0.03	0.021
5978.97	5978.97	Si II	(4)	-0.234	0.02	0.013	0.02	0.017
6046.47	6046.40	O I	(22)	-0.245	0.04	0.029	0.03	0.025
6101.77	6101.80	[K IV]	(1F)	-0.254	0.11	0.085	0.11	0.086
6151.29	6150.90	N II	(36)	-0.262	0.03	0.024	0.03	0.026
6232.13				-0.274	0.06	0.050	0.02	0.013
6300.40	6300.30	[O I]	(1F)	-0.285	3.96	3.048	4.97	3.820
6312.08	6312.10	[S III]	(3F)	-0.287	0.86	0.663	1.04	0.797
6347.14	6347.09	Si II	(2)	-0.292	0.04	0.031	0.05	0.037
6363.85	6363.78	[O I]	(1F)	-0.294	1.38	1.050	1.73	1.316
6371.37	6371.36	Si II	(2)	-0.295	0.04	0.033	0.05	0.036
6461.85		in NGC 7027		-0.309	0.07	0.050	0.06	0.044
6544.53		in NGC 7009		-0.320	0.10	0.076	0.09	0.067
6548.13	6548.03	[N II]	(1F)	-0.321	17.22	12.815	18.45	13.731
6562.80	6562.82	H I	Hα	-0.323	414.00	307.535	377.57	280.475
6577.92	6578.03	C II	(2)	-0.325	0.34	0.254	0.32	0.240
6581.00		in NGC 7009		-0.325	0.10	0.071	0.12	0.086
6583.37	6583.41	[N II]	(1F)	-0.326	50.47	37.389	60.26	44.644
6599.56				-0.328	0.03	0.020	0.03	0.019
6678.18	6678.15	He I	(46)	-0.338	5.27	3.861	5.77	4.223
6716.54	6716.47	[S II]	(2F)	-0.343	0.72	0.528	0.64	0.465
6730.76	6730.85	[S II]	(2F)	-0.345	1.47	1.072	1.64	1.192
6906.41				-0.365	0.02	0.011	0.01	0.010
7002.27	7002.13	O I	(21)	-0.376	0.04	0.027	0.06	0.043
7065.23	7065.28	He I	(10)	-0.383	14.55	10.229	13.77	9.679
7135.83	7135.78	[Ar III]	(1F)	-0.391	22.03	15.374	23.39	16.322
7154.10	7154.10		WR	-0.393	0.297Å	em	0.234Å	em
7160.60				-0.393	0.05	0.036	0.04	0.027
7170.76	7170.62	[Ar IV]		-0.394	0.07	0.049	0.09	0.059

Table 3 – *continued*

$\lambda_{obs'd}$ (1)	λ_{lab} (2)	Element (3)	Mult. (4)	k_λ (5)	F(1990) (6)	I(1990) (7)	F(1991) (8)	I(1991) (9)
7189.37				-0.396	0.01	0.006	0.01	0.009
7231.33	7231.12	C II	(3)	-0.401	0.13	0.089	0.13	0.087
7236.64	7236.19	C II	(3)	-0.401	0.34	0.236	1.49	1.029
7254.58	7254.38	O I	(20)	-0.403	0.04	0.029	0.07	0.048
7263.00	7262.70	[Ar IV]		-0.404	0.07	0.051	0.08	0.055
7281.35	7281.35	He I	(45)	-0.406	1.17	0.803	1.30	0.897
7298.08	7298.05	He I	*	-0.407	0.04	0.030	0.04	0.030
7320.06	7319.65	[O II]	(2F)	-0.410	6.59	4.520	9.06	6.210
7330.22	7330.16	[O II]	(2F)	-0.411	5.42	3.713	7.06	4.838
7468.05	7468.29	N I	(3)	-0.424	0.02	0.012		
7499.88	7499.84	He I	*	-0.428	0.08	0.051	0.08	0.055
7529.94	7529.90	[Cl IV]	(1F)	-0.430	0.15	0.103	0.15	0.102
7751.10	7751.12	[Ar III]	(1F)	-0.451	5.37	3.545	6.27	4.136
7816.17	7816.16	He I	(69)	-0.457	0.12	0.079	0.12	0.079
7876.03	7875.99	[P II]	(3F)	-0.462	0.02	0.013	0.05	0.030
7889.52	7889.90	[Ni III]	(1F)	-0.463	0.01	0.010	0.01	0.006
7896.41				-0.464	0.01	0.009	0.02	0.010
8015.79				-0.474	0.01	0.008	0.01	0.008
8035.04				-0.476	0.01	0.007	0.01	0.009
8045.72	8046.10	[Cl IV]	(1F)	-0.477	0.34	0.218	0.37	0.240
8083.93				-0.480	0.01	0.007	0.01	0.009
8093.32				-0.481	0.01	0.008	0.02	0.011
8203.65				-0.490	0.02	0.013	0.03	0.020
8222.87				-0.491	0.01	0.006	0.01	0.009
8238.60	8238.30	H I	P46	-0.493			0.02	0.012
8240.24	8240.10	H I	P45	-0.493			0.03	0.018
	8242.34	N I	(2)					
8241.96	8242.10	H I	P44	-0.493			0.05	0.029
8243.77	8243.60	H I	P43	-0.493			0.03	0.021
8245.63	8245.70	H I	P42	-0.493	0.04	0.026	0.05	0.032
8247.73	8247.80	H I	P41	-0.493	0.05	0.031	0.06	0.035
8250.04	8250.00	H I	P40	-0.493	0.05	0.034	0.06	0.038
8252.71	8252.50	H I	P39	-0.494	0.05	0.033	0.07	0.042
8255.02	8255.15	H I	P38	-0.494	0.07	0.045	0.07	0.042
8257.87	8257.86	H I	P37	-0.494	0.07	0.042	0.07	0.046
8260.99	8260.94	H I	P36	-0.494	0.09	0.059	0.09	0.058
	8264.57	He I?	*					
8264.43	8264.29	H I	P35	-0.495	0.10	0.064	0.09	0.059
8267.94	8267.94	H I	P34	-0.495	0.09	0.059	0.09	0.058
8271.93	8271.93	H I	P33	-0.495	0.09	0.055	0.09	0.058
8276.36	8276.31	H I**	P32	-0.496	0.10	0.066	0.09	0.056
8281.03	8281.12	H I**	P31	-0.496	0.12	0.075	0.10	0.065
8286.32	8286.43	H I	P30	-0.496	0.13	0.080	0.13	0.083
8292.16	8292.31	H I	P29	-0.497	0.15	0.095	0.13	0.083
8298.79	8298.84	H I	P28	-0.497	0.18	0.111	0.18	0.113
8306.10	8306.12	H I**	P27	-0.498	0.14	0.091	0.20	0.128
8314.42	8314.26	H I	P26	-0.499	0.22	0.137	0.25	0.155
8323.49	8323.43	H I	P25	-0.499	0.25	0.158	0.33	0.205
8333.81	8333.78	H I	P24	-0.500	0.20	0.129	0.26	0.162
8342.50	8342.37	He I	*	-0.501	0.04	0.026	0.07	0.047
8345.46	8345.55	H I	P23	-0.502	0.30	0.192	0.34	0.216
8358.97	8359.01	H I	P22	-0.504	0.31	0.197	0.36	0.226
8361.70	8361.69	He I	*	-0.504	0.16	0.103	0.21	0.134
8374.54	8374.48	H I	P21	-0.506	0.31	0.194	0.35	0.219
8377.01				-0.507	0.02	0.012	0.03	0.017
8392.43	8392.40	H I	P20	-0.509	0.41	0.255	0.42	0.264
8397.46				-0.510	0.02	0.015	0.02	0.010
8413.33	8413.32	H I	P19	-0.512	0.45	0.282	0.43	0.269
8422.08	8422.39	S II?+?	(37)	-0.514	0.02	0.013	0.03	0.018
8433.66	8433.85	[Cl III]**	(3F)	-0.516	0.02	0.015	0.03	0.021
8437.95	8437.96	H I	P18	-0.516	0.47	0.291	0.62	0.386
8444.42	8444.46	Si I?	(46)	-0.517	0.04	0.027	0.07	0.042
8446.53	8446.48	O I	(4)	-0.517	0.34	0.211	0.63	0.390
8451.33	8451.55	S I	(14)	-0.518	0.03	0.018	0.04	0.023
8453.88				-0.519	0.03	0.018	0.03	0.022
8467.24	8467.26	H I	P17	-0.521	0.58	0.358	0.71	0.441
8480.90	8480.85	[Cl III]	(3F)	-0.523	0.03	0.017	0.04	0.024
	8480.73	He I	*					
8486.25				-0.524	0.02	0.015	0.03	0.021
8488.71	8488.77	He I	*	-0.524	0.02	0.013	0.02	0.011
	8488.25	He I	*					
8499.98	8500.00	[Cl III]	(3F)	-0.526	0.03	0.021	0.05	0.031
8502.50	8502.49	H I	P16	-0.526	0.69	0.426	0.76	0.469
8518.01	8518.04	He I	*	-0.528	0.01	0.008	0.02	0.012
8529.10	8528.99	He I	*	-0.530	0.04	0.026	0.06	0.034
8531.48	8531.48	He I	*	-0.530	0.02	0.013	0.02	0.012
8545.29	8545.38	H I	P15	-0.532	0.88	0.540	0.89	0.546
8567.83	8567.74	N I?	(8)	-0.536	0.01	0.006	0.01	0.005
8578.75	8578.70	[Cl II]	(1F)	-0.537	0.14	0.084	0.22	0.136
8582.34	8582.54	He I	*+*	-0.538	0.09	0.057	0.11	0.067

Table 3 – *continued*

$\lambda_{obs'd}$ (1)	λ_{lab} (2)	Element (3)	Mult. (4)	k_λ (5)	F(1990) (6)	I(1990) (7)	F(1991) (8)	I(1991) (9)
8584.58				-0.538	0.03	0.020	0.03	0.016
8598.29	8598.39	H I	P14	-0.540	0.97	0.590	1.13	0.685
8617.65				-0.543	0.03	0.016	0.03	0.016
8648.35	8648.26	He I	*	-0.548	0.05	0.033	0.05	0.033
8650.82	8650.81	He I	*	-0.548	0.02	0.013	0.02	0.012
8665.06	8665.02	H I	P13	-0.550	1.31	0.789	1.26	0.757
8733.53	8733.43	He I	*	-0.560	0.10	0.062	0.08	0.045
8736.09	8736.04	He I	*	-0.560	0.03	0.017	0.03	0.015
8750.48	8750.48	H I	P12	-0.562	1.67	0.996	1.77	1.057
8776.71	8776.77	He I	*	-0.566	0.09	0.051	0.08	0.050
8845.37	8845.38	He I	*	-0.576	0.08	0.050	0.09	0.052
8848.38	8848.05	He I	*	-0.576	0.04	0.021	0.05	0.030
8862.77	8862.79	H I	P11	-0.578	2.10	1.235	2.08	1.224
8914.78	8914.74	He I	*	-0.585	0.02	0.012	0.02	0.012
8996.95	8996.99	He I	*	-0.596	0.11	0.062	0.12	0.068
9014.87	9014.91	H I	P10	-0.599	2.81	1.616	2.98	1.716
9063.37				-0.605	0.09	0.052	0.13	0.072
9069.03	9068.90	[S III]	(1F)	-0.606	9.35	5.354	11.69	6.694
9123.45	9123.60	[Cl II]	(1F)	-0.610	0.03	0.020	0.06	0.033
9210.40	9210.28	He I	(83)	-0.612	0.19	0.107	0.21	0.121
9228.58	9229.02	H I	P9	-0.612	3.66	2.080	3.40	1.937
9463.47	9463.57	He I	(67)	-0.618	0.33	0.188	0.38	0.213
9526.12				-0.620	0.22	0.126	0.14	0.080
9530.71	9531.00	[S III]**	(1F)	-0.620	30.13	17.026	23.50	13.277
9545.96	9545.97	H I**	P8	-0.620	3.35	1.892	2.86	1.618
9603.39	9603.50	He I	(71)	-0.621	0.02	0.012	0.02	0.013
9823.92	9824.11	[C I]	(1F)	-0.627	0.03	0.016		
9850.52	9850.24	[C I]	(1F)	-0.627	0.04	0.021	0.04	0.025
9903.47				-0.628	0.15	0.084	0.20	0.110
9914.31				-0.629	0.04	0.020	0.05	0.026
9945.86				-0.629	0.05	0.030	0.03	0.017
9956.13				-0.629	0.03	0.019	0.03	0.019
10027.67	10027.73	He I	(81)	-0.631	0.28	0.157	0.29	0.162
10031.08	10031.16	He I	(85)	-0.631	0.11	0.060	0.15	0.084
10049.25	10049.38	H I	P7	-0.631	7.59	4.240	8.09	4.523
10123.68				-0.633			0.09	0.048
10286.45	10286.80	[S II]		-0.636			0.35	0.195

*Identification of He I from Osterbrock et al. (1992).
**Lines affected by Earth's atmosphere.
em/abs = equivalent width (Å) for the emission/absorption lines.
? = unlikely or doubtful identification.

listed possible Wolf–Rayet (WR) lines at $\lambda\lambda$4052–63, 4097, 4089, 4542, 4686 and 5807. His description suggests that λ4542 might have had a P Cygni profile. Coudé spectrograms secured at Mt Wilson in 1959 (Aller & Kaler 1964) showed no evidence of any WR features, but thereafter He II 4686 reappeared. Mendez, Manchado & Herrero (1988) noted a recent increase in the stellar He II 4686 line, an effect which they attributed to an increase in the Zanstra temperature from 51 000 to 57 000 K in 20 yr. Actually, the excitation rise occurred on a much shorter time-scale (FAH). The stellar C IV 5801, 5812 lines brightened and the UV spectrum showed complicated changes. Recently, the degree of excitation seems to have levelled off.

Table 4 lists the WR lines observed in the nuclear spectrum of NGC 6572 in 1990 and 1991, with linewidths and central intensities as measured on 1991 August 30. Successive columns give the wavelength, the identification, the overall width in Å of the WR feature, the ratio of the intensity of the line centre to the continuum intensity, and notes. The line profiles are often bell-shaped, but some are irregular, reflecting possible contributions from unresolved, weak lines. He II λ4686 shows a sharp spike (see fig. 16 in FAH), while, for $n \rightarrow 4$ (Pickering series), the spectral spike is inconspicuous. Any He II contribution to Hα, Hβ or Hγ is concealed below strong, nebular H lines. In 1990, He II $\lambda\lambda$5411, 4541 and 4200 showed distinctive P Cygni profiles but, by 1991, the P Cygni absorptions seemed to be lost under emission.

4 INTERPRETATION OF LINE INTENSITIES

4.1 Diagnostic lines and ionic concentrations

In comparison with other PNe which show a smaller variety of ionic lines with often only relatively strong lines being measurable, NGC 6572 shows a rather rich spectrum. We

Table 4. Wolf–Rayet lines in the optical spectrum of NGC 6572, as measured on 1991 August 30.

λ(Å) (1)	Ident. (2)	Δλ(Å) (3)	I_m/I_o (4)	Notes (5)	λ(Å) (1)	Ident. (2)	Δλ(Å) (3)	I_m/I_o (4)	Notes (5)
4089	——	4.7	1.08		4621	NV	4	1.12	
4097	NIII+	10	1.1:	(a)	4642	NIII	7	1.11	
4129	——	1.8	1.07	(b)	4658	CIV	3.7	1.2	
4132	——	3	1.11		5411	HeII	2.5:	1.25	(c)
4200	HeII			(c)	5801	CIV	6.5:	2.0	(e)
4541	HeII	5:	1.12	(c)	5812	CIV	6:	1.9	(e)
4604	NV	6	1.15	(d)					

Notes. The overall widths Δλ(Å) are difficult to measure in some of these features because of uncertainty in placement of the continuum level. (a) Difficult to estimate because of strong overlying nebular lines; (b) these appear to be distinct lines; (c) P Cygni profiles were seen in 1990; (d) irregular profile; (e) see FAH for profile variations up to 1990.

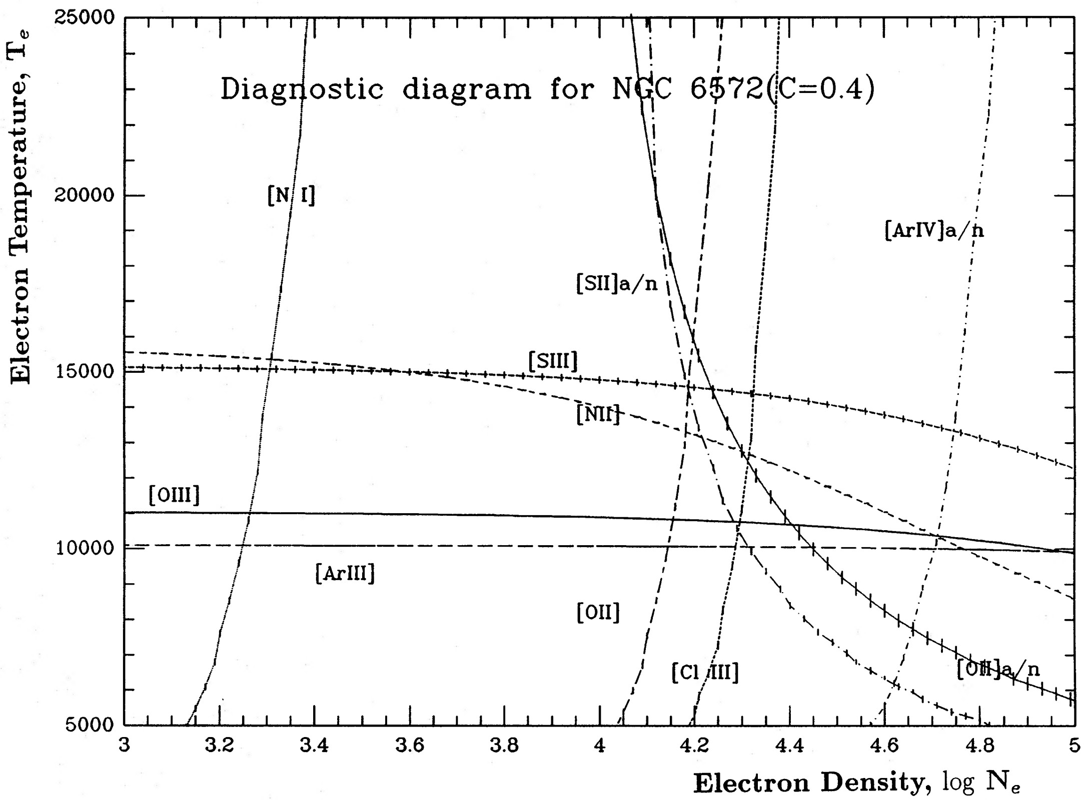

Figure 3. Diagnostic diagram for NGC 6572. The ratios of nebular-type transitions in p^3 configurations of [N I], [O II] and [Cl III] depend mostly on N_e, but the auroral/nebular-type transitions in O^+ and S^+, denoted as [O II]a/n and [S II]a/n, are sensitive to both T_e and N_e. The well-known auroral/nebular-type transitions such as λ4363/λ5007 in [O III] or λ5755/λ6584 in [N II] depend primarily on T_e until N_e exceeds 10 000 cm^{-3}.

want to exploit these data to obtain not only the mean values of the electron temperature and density but also the value of their fluctuations, as these quantities are very important for abundance determinations (Peimbert 1967). NGC 6572 would appear to offer some unique opportunities.

From the measured line intensities as corrected for interstellar extinction with $C=0.4$, we construct the diagnostic diagram shown in Fig. 3. Curves labelled a/n indicate the use of ratios of auroral to nebular-type transitions. The [N I] lines presumably originate in neutral blobs of low electron density. The curve for [S III] based on $[I(9532)+I(9069)]/I(6312)$ is suspect because of the effects of terrestrial water vapour absorption. The best choice for the electron temperature would appear to be near 11 000 K, and the best choice for N_e to be about 20 000 electron cm^{-3}.

Table 5 gives the fractional ionic concentrations, which can be calculated from the observed line intensities once the appropriate N_e and T_e are specified. The columns are self-

Table 5. Fractional ionic concentrations for NGC 6572.

Ion	Lines	I_{corr}	T_ϵ	$\frac{N(i)}{N(H^+)}$	$\Sigma\frac{N(i)}{N(H^+)}$
He I	6678	3.86	10000.	0.1001	
He I	4471	5.30	10000.	0.1022	
He I	5876	16.93	10000.	0.1080	
He II	4686	0.38	11000.	0.0003	
He II	5412	0.00	11000.	0.0000	0.1054
C II	2325,2329	20.82	10000.	3.26E-05	
C III	1907,1909	103.[b]	11000.	1.35E-04	1.67E-04
N I	5198,5200	0.18	10000.	8.90E-07	
N II	6548/84,5755	51.66	10000.	9.40E-06	
N III	1747-1754	5.66	11000.	3.66E-05	4.69E-05
O I	6300/63	4.10	10000.	4.34E-06	
O II	3727,7319/30	25.11	10000.	3.30E-05	
O III	1658,1666	6.18	11000.	1.45E-04	(×)
O III	4959,5007,4363	1488.02	11000.	3.07E-04	3.44E-04
Ne III	3868,3967	125.68	11000.	5.49E-05	5.49E-05
Si III	1884,1892	1.73	11000.	5.21E-07	5.21E-07
S II	6717/31,4068/7	3.53	11000.	1.51E-07	
S III	6312	0.66	13000.	5.21E-07	
S III	9069,9352	22.38	13000.	5.09E-07	
S IV	10.5μm	27.30	13000.	1.35E-06	2.02E-06
Cl III	5517,5537	0.53	11000.	3.91E-08	
Cl III	8481,8501	0.04	11000.	4.33E-08	
Cl IV	7530,8045	0.32	13000.	1.21E-08	5.33E-08
Ar III	7135,7751	18.92	10000.	1.29E-06	
Ar III	5192	0.10	10000.	1.23E-06	
Ar IV	4711,4740	3.15	10000.	3.78E-07	
Ar IV	7265/40,7173	0.10	10000.	8.01E-07	1.85E-06
K IV	6103	0.09	13000.	1.23E-08	
K V	4122,4163	0.02	13000.	4.01E-09	1.63E-08
P II	7876,11883,11468	0.713	11000.	2.86E-09	2.86E-08

[a]From Boggess, Feibelman & McCracken (1981).
(×) Ignored because of its relatively weak intensity.

explanatory; we chose $N_e=24\,000$ electron cm^{-3} throughout, although lower values are more likely for [N I] and [O I]. The C III 1549, 1551 lines are a composite of stellar and nebular contributions; we cannot use them to calculate $N(C^{++})/N(H^+)$. The theoretical model discussed in Section 5 is used as a guide in the choice of electron temperatures. The ionization correction factors (ICFs) are calculated from the final model and used to derive N(total) from ΣN(ion)/$N(H^+)$.

4.2 The helium spectrum

Smits (1991) has calculated the relative intensities for the recombination spectrum of He I for a range of electron densities, viz., 10^2, 10^4 and 10^8 cm^{-3}, and temperatures including 5000, 10 000 and 20 000 K. His treatment resembles that of Brocklehurst (1972). Smits includes angular-momentum-changing collisions of type $nl \rightarrow nl \pm 1$, and energy-changing collisions of type $nl \rightarrow n'l \pm 1$. He also takes into account collisional ionization. Self-absorption from the metastable 2^1S and 2^3S levels are not considered, but collisional effects from these levels are taken into account.

In their classical investigation, Baker & Menzel (1938) described two alternative hypotheses of nebular H-line excitation. In case A, an atom enters a level n, either by electron capture from the continuum or by cascade from a higher discrete level. The stellar radiation field is neglected, and it is assumed that there is no reabsorption of Lyman-line radiation. If the nebular is very opaque to Lyman-line radiation, and if we neglect the stellar Lyman-line radiation, we can assume that absorptions from levels 1 to n are exactly balanced by the inverse spontaneous transitions. This situation is denoted as case B. Cases A and B may be applied to other atoms, such as He I, C, N, O, etc.

In Table 6, we compare observed values of $I^*(\lambda)=I(\lambda)/$ I(4771) with theoretical predictions by Smits for $T_e=10\,000$ K and $N_e=10^4$ cm^{-3}. The predicted values change slowly with N_e in this range. There is no consideration of collisional effects other than those treated by Smits,

Table 6. The helium spectrum of NGC 6572.

n		I^*_{pred}	I^*_{obs}	n		I^*_{pred}	I^*_{obs}
	2^3P – n^{3}D				2^1P – n^{1}S		
3	5875.67	2.68	3.02	3	7281.35	14.5(-2)	15.6(-2)
4	4471.51	1.00	1.00	4	5047.74	4.08	3.35
5	4026.36	0.486	0.463	5	4437.55	1.70	1.82
6	3819.61	0.266	0.225	6	4165.97	0.90	1.25
7	3705.02	0.178	0.132	7	4024.0	0.59	0.63
	2^3P – n^{3}S				2^1P – n^{1}D		
3	7065.28	0.464	1.83	3	6678.15	0.767	0.743
4	4713.14	0.115	0.138	4	4921.93	0.220	0.261
5	4120.81	0.0416	0.061	5	4387.93	0.129	0.123
6	3867.63	0.0213	0.025	6	4143.76	0.0723	0.071
7	3733.00	0.0124	0.011				
					3^1S – n^{1}D		
	3^3D – n^{3}F			6	9603.50	0.556(-2)	0.23(-2)
7	10031.16	4.71(-2)	1.3(-2)	7	8914.74	0.428	0.21
11	8848.0	1.10	0.45	8	8518.74	0.286	0.15
12	8736.04	0.8414	0.30				
13	8650.81	0.658	0.23		3^1D – n^{1}F		
15	8531.48	0.425	0.15	7	10027.73	1.57(-2)	2.95(-2)
				9	9210.54	0.693	2.1
	3^3S – n^{3}P			10	8997.03	0.496	1.09
5	9463.57	2.56(-2)	3.65(-2)	11	8845.38	0.368	0.92
7	7816.16	1.16	1.45	12	8133.43	0.281	0.30
8	7499.84	0.787	0.98	13	8650.51	0.22	0.5
9	7298.05	0.560	0.55	14	8529.0	0.14	0.5:
	3^3P – n^{3}D						
9	8776.77	0.948(-2)	0.98(-2)				
10	8582.54	0.755	1.15				

$I^*(\lambda) = I(\lambda)/I(4471)$.

and there is no allowance for optical-depth effects, which may be important for λ7065 in the 2^3P–n^3S series. Although the agreement between theory and observation varies from one series to another, there seems to be no indication of any systematic error in our measured line intensities. For the 2^3P–n^3D (λ5876 etc.) series there appears to be a reasonable agreement, although the higher members are weaker than predicted. Turning to the triplet series terminating on the $n=3$ levels, we note that, except for λ7298, $I^*_{\text{pred}} \sim 0.8\ I^*_{\text{obs}}$ for the 3^3S–n^3P series. Only two lines are observed for the 3^3P=n^3D series; λ8777 shows good agreement, but λ8582 does not. Note that, for 3^3D–n^3F, the predicted values exceed the observed ones by nearly a constant factor of 2.8. Turning to the singlet series, we find good agreement for the 2^1P–n^1S (λ7281 etc.) series and for the 2^1P–n^1D ($\lambda\lambda$6678 and 4921 etc.) series, but that, for 3^1S–n^1D, the predicted intensities are about twice the observed ones. The agreement for 3^1D–n^1F is poor.

An attempt to explain these discrepancies lies outside the scope of this paper. Water vapour absorption may affect some of these lines. A detailed study would be very difficult. We have measured He I lines with the Hamilton echelle spectrograph in several PNe: an attack on the problems employing the whole body of nebular data might prove more useful than employing NGC 6572 data only.

4.3 Permitted ionic lines of C, N and O

Several PNe of high surface brightness show permitted lines of C, N, O and occasionally Ne. These emissions are often regarded as recombination features. If we accept this hypothesis, we may analyse many of the observed lines with the aid of recombination coefficients given by Pequinot, Petitjean & Bonisson (1991). Table 7 summarizes the results. The C III ionic concentration with respect to H, $0.48 \pm 0.2(-3)$, given by the C II $\lambda\lambda$4267, 6578 and 7231 lines, which presumably arise from recombination, is larger than that found from the collisionally excited C III] 1907/09 lines, $0.135(-3)$. We assumed the T_e values given in Table 5. If we assume that both the C II and C III lines are produced in strata at the same T_e, we find that for $T_e \sim 9500$ K the two sets of carbon ionic lines give an accordant value, $N(C^{++})/N(H^+) \sim 0.41 \times 10^{-3}$. The weighted mean value of $N(C^{+3})/N(H^+)$ found from the C III 4187 and 4647 lines, namely $0.14 \pm 0.06(-4)$, is less than that found from the theoretical model to be described in Section 5. The C IV 1548/51 line shows a P Cygni profile; the stellar and nebular contributions cannot be disentangled.

From the N II multiplets 5, 39 and 59, we find $N(N^{+2})/N(H^+) \sim 0.31 \pm 0.03(-3)$, while the model gives $0.30(-3)$. The only N III line we can use is λ4379, since $\lambda\lambda$4101 and

Table 7. Recombination-line interpretation.

	Mult.	Case B	Case A	Notes	Ref.
OII	(1)	0.69(-3)	0.71(-3)		PSTP
	(5)	0.58(-3)	0.57(-3)		PPB
	(10)		0.87(-3)		PPB
	(2)	0.46(-3)	0.59(-3)		PPB
	(54)		0.62(-3)		PPB
	(67)		0.72(-3)		PPB
	(48)		0.47(-3)		PPB
$N(O^{++})/N(H^+)$	(1),(2),(5),(10)	0.62(-3)	0.75(-3)	mean	PSTP
$N(O^{++})/N(H^+)$		0.52(-3)	0.64(-3)	mean	PPB
$N(O^{++})/N(H^+)$		0.31(-3)			Table 5
CII	(6)	0.42(-3)			
	(3)	0.30(-3)			
	(2)	0.10(-2)			
$N(C^{++})/N(H^+)$		0.48±0.2(-3)		mean	
$N(C^{++})/N(H^+)$		0.135(-3)			Table 5
CIII	(21)		0.097(-3)		
	(1)		0.178(-3)		
$N(C^{+++})/N(H^+)$			0.14±.06(-4)	mean	
$N(C^{+++})/N(H^+)$		0.30(-3)			model
NII	(5)	0.30±.03(-3)	0.38(-3)		
	(59)	0.38(-3)			
	(39)	0.31(-3)			
$N(N^{++})/N(H^+)$		0.31±.03(-3)		mean	
$N(N^{++})/N(H^+)$		0.30(-3)			Table 5
NIII	(17)	0.32(-4)			
$N(N^{+++})/N(H^+)$	(17)	0.32(-4)		mean	
$N(N^{+++})/N(H^+)$		0.24(-4)			model

PSTP: Peimbert, Storey & Torres Peimbert (1993).
PPB: Pequinot, Petitjean & Bonisson (1991).
model: see Section 5.

4641 are excited by fluorescence. This line gives $N(N^{+3})/N(H^+)=0.32(-4)$, while the model gives 0.24(−4).

Several lines of multiplets 20–25 of O I are observed, but no recombination predictions are available. The strongest O I line is λ8446. From a measurement of the relative strengths of λλ13164 and 8446, and from the absence of λ11287, Rudy et al. (1991) conclude that λ8446 and other O I lines are excited by fluorescence from the stellar continuum, and that Lyβ plays no important role.

There are numerous permitted O II lines. Peimbert, Storey & Torres Peimbert (1993, hereafter PSTP) employed Storey's recombination coefficients to analyse multiplets 1, 2, 5 and 10 to obtain $N(O^{++})/N(H^+)$. They used empirically corrected O II photographic line intensities measured by Aller & Kaler (1964) to find a recombination-theory-based estimate of $N(O^{++})/N(H^+)$. Then, by comparing this result with the $N(O^{++})/N(H^+)$ value obtained from the collisionally excited [O III] lines, they derived a value of 0.04 ± 0.025 for Peimbert's (1967) temperature fluctuation parameter t^2. We have employed our own echelle measurements, given in Table 3, with the Pequinot et al. (1991) recombination coefficients, and also with the PSTP data (cf. their tables 1 and 7). These are denoted as PPB in our Table 7. Then, by comparing the $N(O^{++})/N(H^+)$ values derived via the recombination hypothesis with those found from the [O III] lines, we find the former to be the larger. The discrepancy is qualitatively similar to that found for the C^{++} abundances derived from λλ4276 and 1908, respectively, as noted above.

Electron temperature difference between the regions where O II and [O III] emissions, respectively, are favoured may explain the discordances. An application of the Peimbert theory to our present observations suggests that $t^2\sim0.055$, which seems rather high. Photometric errors cannot be blamed. Fluorescence seems unlikely for the O II lines in NGC 6572. If it was important, we would expect different O II lines to give noticeably different values of $N(O^{++})/N(H^+)$; this does not appear to be the situation.

5 THEORETICAL MODEL FOR NGC 6572

We determine the chemical composition of NGC 6572 by two procedures: (a) compute the concentration of each ion using T_e, N_e and appropriate atomic constants, and then deduce the total elemental abundances by multiplication by the appropriate ICF; (b) represent the line intensities by the model, and accept that abundance as appropriate for the element involved. Both procedures have often been used in the past.

A spherically symmetrical shell model is certainly not appropriate for NGC 6572, even in the first approximation. The VLA maps presented by Masson (1989) and by Basart & Daub (1987), and the IR images by Hora et al. (1990) showed that NGC 6572 is limb-brightened on the minor axis and has sharp edges to the ionized regions, which must be surrounded by neutral material. To reproduce the general structure of NGC 6572, Masson (1989) constructed an ellipsoidal shell model which consists of inner boundaries, 1.45×5.09 arcsec^2, and outer boundaries, 2.60×6.24 arcsec^2. The shell is assumed to be tilted at an inclination angle of $i = 50°$. Using this shell model, Masson (1989) calculated the correction factor needed to derive the kinetic motions from observed apparent angular displacements. Thus he was able to interpret the angular expansion of the nebula, eventually to obtain the distance of NGC 6572 as $1.7^{+6.1}_{-0.8}$ kpc. Ellipsoidal shell models for PNe have been proposed often, e.g. by Atherton et al. (1978) and Balick, Preston & Icke (1987).

More recently, Masson (1990) has proposed a model which is very successful in reproducing the general appearance of a limb-brightened nebula such as NGC 6720, 7027 or 6572. He assumed an idealized nebular structure consisting of a closed hollow shell, surrounded by neutral material. Assuming that the nebular structure has a prolate shape, and that the inner surface radii of the ionized regions at the polar and equatorial shells are given, the photoionization-limited outer boundary can be calculated. By invoking a modest degree of asymmetry in the material, and by trying different inclination angles, we can reproduce many of the observed axisymmetrical PN shapes.

As Masson (1990) pointed out, however, this proposed model is deficient in several respects. For example, there is no allowance for T_e and N_e variations with distance from the central star. Furthermore, the simple model does not represent an exact solution of the appropriate equations of statistical equilibrium and radiative transfer. The prolate model by Masson (1990) assumes that a PN has an ionization-bounded shell. With a thick nebular shell, such a model might fail to reproduce the limb/central brightness contrast. None the less, Masson's model seems to be generally successful in depicting many of the bilaterally symmetrical nebulae.

Cylindrical shell models have also been proposed as idealizations, recently for example by Hora et al. (1990), but such ad hoc structures cannot be easily reconciled with any reasonable hypothesis about the origin and evolution of PNe. Thus we shall not consider them here.

The density-contrast model (see, e.g., Clegg et al. 1987; Hyung 1994) avoids some of the difficulties of a single prolate-shell configuration. An axially symmetrical PN is assumed to comprise an equatorial toroid with one density distribution and a cone with yet another. In IC 2149, for example, the nebular image in one ionization stage, e.g. [O II], is quite different from that in the next ionization stage, [O III]. With a density-contrast model this behaviour can be regarded as a projection effect (Feibelman, Hyung & Aller 1994), while an ellipsoidal model fails. We employ a photoionization-model approach wherein energy and statistical balance equations are explicitly satisfied. One is concerned not only with nebular shapes, but also with their spectra. Preliminary calculations showed that the structure of NGC 6572 could be understood in terms of density-contrast geometry. An account of the methods of computation, atomic constants employed, etc. is found in Hyung (1994). We also updated the atomic data for [S II], supplied by Keenan et al. (1993). The newly improved atomic constant

Table 8. Details of the final model.

Adopted distance =1500pc (Hajian, Terzian, & Bignell ,in preparation)

Equatorial shell density =25000 cm^{-3}	**R(inner), R(outer)** = 0.01, **0.0244pc**
Polar conic shell density =16000 cm^{-3}	**R(inner), R(outer)** = 0.024, **0.0362pc**
Equatorial (latitude) angle, 2A = 90°	**Inclination angle,** i = 40°
Observed <T$_e$>≃ 10900K([OIII],slit)	**Predicted <T$_e$>= 10940K([OIII],slit)**
Central star	
Hubeny model, He/H = 0.10	**L(⋆)**= 3820**L(⊙)**
Radius = 0.823 R(⊙)	**T(⋆)**= 50000**K, log g** = 5.5

Observed F(Hβ)≃ 3.83 × 10^{-10} ergs·cm^{-2}·s^{-1} (Acker et al. 1992)
Predicted F(Hβ)≃ 3.98 × 10^{-10} ergs·cm^{-2}·s^{-1}

Assumed Abundances

He	C	N	O	Ne	S	Ar	Cl
9.30E-02	1.35E-04	9.60E-05	3.10E-04	5.50E-05	3.40E-06	2.00E-06	6.00E-08
P	**Na**	**Ca**	**Mg**	**F**	**K**	**Si**	
7.00E-07	2.10E-08	7.50E-08	1.00E-08	1.00E-08	2.00E-08	1.90E-06	

for [S II], however, gives minor variance in the prediction of line intensities (~ 2 per cent). In the preliminary models, we used Hubeny's (1988) non-LTE atmospheres for $T_{\rm eff}=70\,000$, 60 000 and 50 000 K, with log $g=5.5$ and He/H = 0.10. First, we calculated models with various homogeneous shells of densities 25 000, 20 000, 15 000 and 10 000 atom cm^{-3}. We also tested a model in which the shell density decreased inversely as a function of radius, e.g. 35 000 r^{-2}. We checked model predictions for both ionization-bounded and material-bounded cases. It soon became evident that models with the Hubeny $T_{\rm eff}=70\,000$ K atmospheres predicted too high a level of excitation, while models with $T_{\rm eff}=50\,000$ and 60 000 K seemed to yield predictions close to the observations. To handle the nebular structure and spectroscopic data, a density-contrast model seemed necessary, the density in the equatorial shell being greater than that in the cone.

After laborious trials, we adopted an energy distribution corresponding to a $T_{\rm eff}=50\,000$ K Hubeny model atmosphere with log $g=5.5$. We adopted a distance of 1.5 kpc (using the expansion parallax algorithm method by Hajian, Terzian & Bignell 1993, in preparation). Table 8 summarizes the data for the final model. We take $R(\star)=0.823$ R$_{\odot}$; then $L(\star)=3820$ L$_{\odot}$. The hydrogen densities of the polar and equatorial shells are 16 000 and 25 000 atom cm^{-3}, respectively. The toroidal equatorial belt is taken as a ring with an inner radius of 0.01 pc and an outer radius of 0.0244 pc. The polar conical shell is assumed to have an inner radius of 0.024 pc and an outer radius of 0.0362 pc; both shells are radiation-bounded.

In order to reproduce the nebular shape observed by Masson (1989, 1990), we must select the extent in latitude for the toroidal ring and the spatial orientation of the symmetry axis. We assume that the equatorial ring extends from 'latitude' of $-45°$ to $+45°$, and that the symmetry axis is tilted at an inclination axis of 40°. Schematic representation of the model for NGC 6572 is diagrammatically shown in Fig. 4. The predicted contour in Hβ from the final model is also presented in Fig. 5(a), which can be compared with an observed nebular appearance, e.g., a recently observed radio image (Masson 1989) shown in Fig. 5(b).

An essential step in the analysis is to compare predicted with observed line intensities, taking into account the fact that intensity measurements with different techniques refer to different regions of the image. The *IUE* data were all obtained with an elliptical slot, while all optical region data were secured with a slit 1.14 × 4 arcsec^2 on the Hamilton spectrograph. Because of image rotation and seeing, the effective size of the slot on the image in a typical exposure can be 2 × 4 arcsec^2, or even larger.

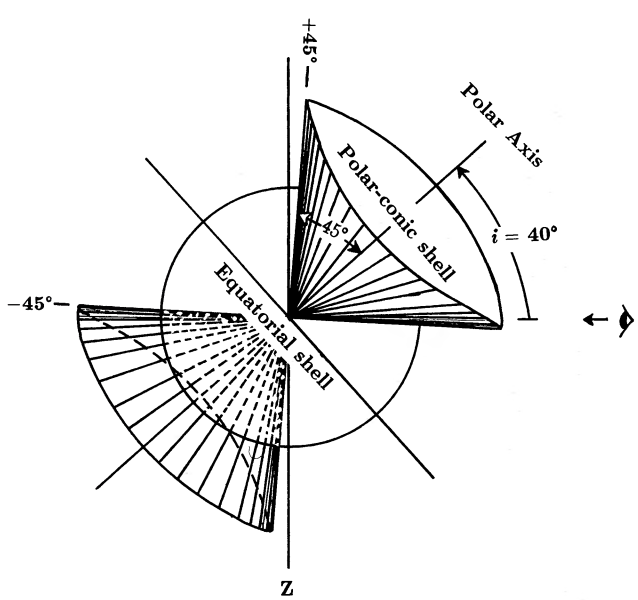

Figure 4. Schematic sketch of the density-contrast model for NGC 6572, showing an orientation relative to the observer. The Z-axis is in the plane of the sky. See text for the exact physical size of each shell.

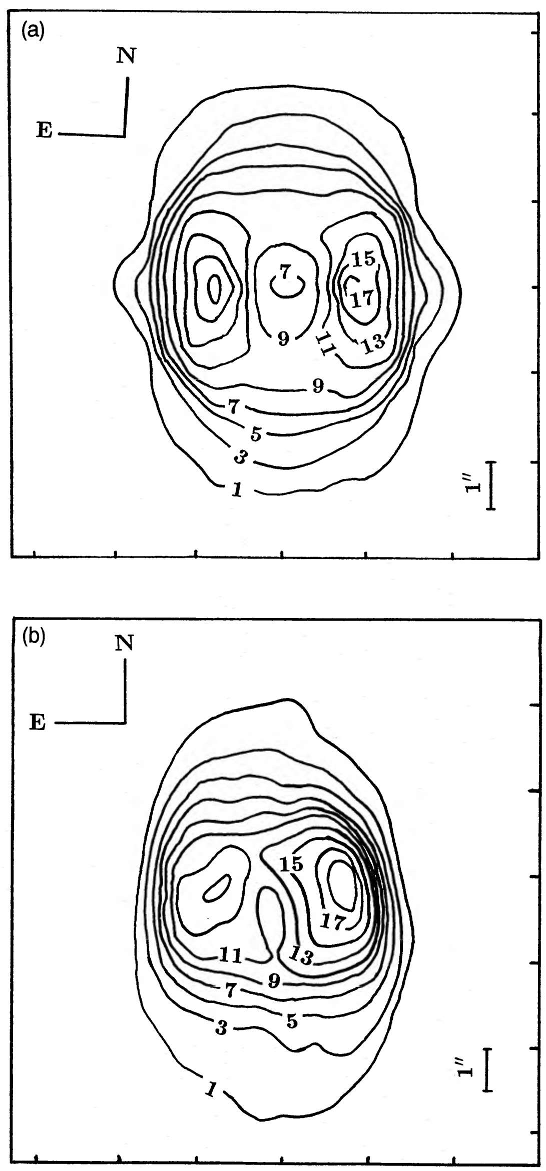

Figure 5. Normalized surface brightness contours: (a) predicted Hβ map from the final model; (b) observed VLA CLEAN map at 4.885 GHz (Masson 1989).

Table 9. Comparison of observed and predicted intensities in NGC 6567.

El Ion (1)	λ(Å) (2)	I_{obs} (3)	I_{cal} (4)	El Ion (1)	λ(Å) (2)	I_{obs} (3)	I_{cal} (4)
He I	5876	16.90	15.14{15.44}	Ne III	3868	95.3	95.65{107.7}
He I	6678	3.86	3.92{3.93}		3969	30.4	28.59{32.11}
He I	4471	5.30	5.18{5.32}				
				Si III	1883\	0.965	{0.27}
C II	2325\	11.82	{2.22}		1892/	0.764	{1.99}
	2328/	9.00	{22.13}				
	4267	0.46	0.07{0.07}	S II	4068	1.34	0.89{2.04}
C III	1907\	–	{42.80}		4076	0.59	0.30{0.69}
	1909/	103.[a]	{45.62}		6717	0.53	0.51{1.15}
C IV	1548\	–	{19.42}		6731	1.1	1.00{2.25}
	1551/	–	{9.86}	S III	6312	0.7	0.60{1.01}
					9069	5.4	8.84{14.13}
N II	6584	37.2	37.37{79.16}		9531	16.9	21.59{34.47}
	6548	12.8	12.90{27.32}	S IV	10.5μm	27.3[b]	36.90[c]
	5755	1.50	1.32{2.85}				
N III	1747-54	5.66	{11.90}	Cl II	8580	0.084	0.05{0.10}
	2754	–	{1.16}	Cl III	5518	0.16	0.09{0.12}
					5538	0.38	0.25{0.32}
O I	6300	3.0	2.21{5.23}	Cl IV	7530	0.10	0.15{0.13}
	6363	1.0	0.70{1.67}		8046	0.22	0.34{0.30}
O II	3726\	16.8	16.10{33.79}				
	3729/	6.5	6.09{12.78}	Ar III	5193	0.10	0.09{0.15}
	7321/2\	4.50	4.37{9.17}		7136	15.37	8.86{14.99}
	7332/3/	3.7	3.51{7.36}		7751	3.55	2.15{3.63}
O III	1660	1.81	{4.77}		9.0μm	11.5[b]	8.9[c]
	1666	4.36	{11.71}	Ar IV	4711	0.90	4.63{4.03}
	4363	8.3	10.01{11.45}		4740	2.26	11.29{9.42}
	4959	372.	363.2{377.5}		7238	–	0.12{0.10}
	5007	1107	1047{1087}		7265	0.05	0.13{0.11}
					7172	0.05	0.16{0.14}
P II	11883	0.46[d]	0.40[c]				
	11468	0.24[d]	0.17[c]	Mg II	2796	–	{0.05}
	7876	0.013	0.014		2804	–	{0.02}

$I_{\rm obs}$ of *IEU* region in column (3) and $\{I_{\rm cal}\}$ in column (4): integrated intensities over a whole PN.
$I^{a}_{\rm obs}$, $I^{b}_{\rm obs}$ and $I^{d}_{\rm obs}$ in column (3) are from Boggess et al. (1981), Beck et al. (1981) and Rudy et al. (1991), respectively [I(Hβ) = 100].
$I^{c}_{\rm cal}$ in column (4) from using a slit size 6.5 × 6.5 arcsec^2.

Table 9 compares, in columns (3) and (4), predicted and observed intensities for our models. We list predicted intensities both for a 2 × 4 arcsec^2 slot, corresponding to the Hamilton observations, and for a large slot, e.g. 12 × 12 arcsec^2 (or integrated over the whole nebular volume), corresponding to the observations over the whole nebular image, all on the scale I(Hβ) = 100. The latter are indicated by { } in column (4). Photoelectric scanner measurements by Peimbert (1967) and others give the monochromatic fluxes for the stronger lines over the entire nebular image. Likewise, the *IUE* data and IR measurements of [Ne II] and [S IV] pertain to the entire image, so the proper predicted intensities for these data are the bracketed values ({ }). We choose the 1990 Hamilton data for comparison with the unbracketed predicted values in column (4). Discrepancies between model predictions and observations must arise largely from geometrical effects or irregularities in the nebular structure. Note the large difference between the predicted slot and total intensities for [N II] and [O II]. The difficulties in determining the phosphorus abundances are coming not only from uncertainties in the atomic parameters but also from the absence of observable ionization states other than P^+. Although there are two observable [P II] lines (λλ7876 and 4669) in the Hamilton spectroscopic data, [P II] 4669 seems to be blended with a relatively strong [O II] line. We also used the two near-IR spectroscopic data, [P II] 11468 and 11883 lines, by Rudy et al. (1991). Based on the above two IR lines and using the Czyzak et al. (1968) and Wiese, Smith & Miles (1969) atomic data, Rudy et al. (1991) estimated the total phosphorus abundance as N(P)/N(H) = 3.63(−7). When we applied their phosphorus abundance, the model which employed the more recent compilation predicted the line intensities to be ~50 per cent of the observed. Thus we adopted the phosphorus abundance as N(P)/N(H) = 7(−7) in the model calculation (see also the ICF-method result in Table 10).

Table 10. Relative chemical abundances for NGC 6572.

Element	$\Sigma \frac{N(i)}{N(H^+)}$	ICF	ICF Method	Model	Δ	Sun*
He	1.1054	1.00	1.1054	0.930	0.08	0.098
C^w	1.67E-4	1.282	2.14E-4	1.35E-4	0.20	3.6E-4
N	4.69E-5	1.323	6.20E-5	9.60E-5	-0.19	1.1E-4
O	3.44E-4	1.000	3.44E-4	3.10E-4	0.05	8.5E-4
Ne	5.49E-5	1.038	5.70E-5	5.50E-5	0.02	1.2E-4
Si^w	5.21E-7	3.650	1.90E-6	1.90E-6	0.00	3.5E-5
P^w	2.86E-8	22.22	6.35E-7	7.00E-7	-0.04	2.8E-7
S	2.02E-6	1.067	2.16E-6	3.40E-6	-0.20	1.6E-5
Cl	5.33E-8	1.266	6.75E-8	6.00E-8	0.05	3.2E-7
Ar	1.85E-6	1.021	1.89E-6	2.00E-6	-0.02	3.6E-6
K	1.63E-8	1.172	1.91E-8	2.00E-8	-0.02	1.3E-7

[w]The ICFs for these elements pertain to the whole nebular image.
*Solar abundances by Grevesse & Anders (1989).

Table 10 compares relative chemical abundances for NGC 6572 as derived by the ICF and model methods with the solar values by Grevesse & Anders (1989). The nebular N abundances are only slightly lower than the solar values; for other elements the nebular abundances are substantially lower. If we adopt temperature fluctuations of the type suggested by Peimbert (1967), the abundances of all elements represented by collisionally excited lines will be enhanced by an amount that differs from element to element and depends on the t^2 parameter (see Zuckerman & Aller 1986 for illustrative examples).

NGC 6572 may have evolved from a star in which the metal/H ratio was initially between 40 and ≥ 100 per cent of that of the Sun, depending on our choice of the Peimbert t^2 parameter. N was later enhanced. Taking $L(\star)$ and $T(\star)$ at their face values and utilizing Schonberner's (1981) evolutionary tracks, we derive a core mass of about 0.569 $M_\odot$, corresponding to a progenitor star of about 1 $M_\odot$. The evolutionary track would suggest an age between 6000 and 8000 yr. If we assume that the distance of NGC 6572 is 2 kpc instead of 1.5 kpc, we would find an evolutionary age closer to 2500 yr. With an expansion velocity of 16 km s^{-1} and a distance of 2 kpc, our assumed nebular radii imply an age of about 2600 yr.

In conclusion, we mention that NGC 6572 presents some intriguing mysteries. First, as regards the central star, its spectrum may have a cycle of the order of 70 yr. Wright's description of WR-type features roughly matches what we observed in 1986–1992, while in 1959 the spectrum was free of prominent emission features. As opportunities permit, we plan to continue to monitor this star. A more accurate parallax of this object would enable us to define more precisely the character of the central star.

High-resolution direct imaging of the nebula will enable us to assess its inhomogeneities, and the character of low-excitation blobs such as those of [N I]. Kinematic measurements, such as those obtainable with the VLA, should enable us to construct time-dependent models for NGC 6572 – the next step in our theoretical programme.

ACKNOWLEDGMENTS

The ground-based observational aspects of this programme were supported in part by National Science Foundation Grant AST 90-1433 to UCLA, while the UV observations with the *International Ultraviolet Explorer* satellite were supported in part by National Aeronautics and Space Administration Grant NAG 5-1207 ADF to UCLA. We thank Dr Ivan Hubeny for a copy of his model-atmosphere program, which has been applied to our theoretical nebular investigation. We are grateful to Dr Manuel Peimbert, who supplied us with a preprint of work on recombination lines of O II (PSTP, cited above), and to Dr F. P. Keenan, who sent us results of some new atomic calculation for S II.

REFERENCES

Acker A., Ochsenbein F., Stenholm B., Tylenda R., Marcout J., Schohn C., 1992, Strasbourg – ESO Catalogue of Galactic Planetary Nebulae. European South Observatory, Garching bei München
Aller L. H., Kaler J. B., 1964, ApJ, 140, 621
Atherton P. D., Hicks T. R., Reay N. K., Worswick S. P., Hyden Smith W., 1978, A&A, 66, 297
Baker J. G., Menzel D. H., 1938, ApJ, 88, 52
Balick B., Preston H. L., Icke V., 1987, AJ, 94, 1641
Basart J. P., Daub C. T., 1987, ApJ, 317, 412
Beck S. C., Lacy J. H., Townes C. H., Aller L. H., Geballe T. R., Baas F., 1981, ApJ, 249, 592
Boggess A., Feibelman W. A., McCracken C W., 1981, in Chapman R., ed., The Universe at Ultraviolet Wavelengths: The First Two Years of IUE, NASA Conf. Publ. 2171, 663
Brocklehurst M., 1972, MNRAS, 157, 211
Cassatella et al., 1990, NASA *IUE* Newsletter, 41, 155
Clegg R. E. S., Harrington J. P., Barlow M. J., Walsh J. R., 1987, ApJ, 314, 551
Czyzak S. J., Krueger T. K., Martins P. de A. P., Saraph H. E., Seaton M. J., Shemming J., 1968, in Osterbrock D. E., O'Dell C. R., eds, Planetary Nebulae. Reidel, Dordrecht, p. 138
Feibelman W. A., Aller L. H., Hyung S., 1992, PASP, 104, 339 (FAH)

Feibelman W. A., Hyung S., Aller L. H. 1994, ApJ, 426, 653
Grevesse N., Anders E., 1989, in Waddington J., ed., Cosmic Abundances in Matter. American Institute of Physics, New York, p. 1
Hora J. L., Deutsch L. K., Hoffmann W. F., Fazio G. G., 1990, ApJ, 353, 549
Hubeny I., 1988, Comput. Phys. Comm., 52, 103
Hyung S., 1994, ApJS, 90, 119
Hyung S., Aller L. H., Feibelman W. A., 1993, PASP, 105, 1279
Keenan F. P., Hibbert A., Ojha P. C., Conlon E. S., 1993, Phys. Scr., 48, 129
Masson C. R., 1989, ApJ, 346, 243
Masson C. R., 1990, ApJ, 348, 580
Mendez R. H., Manchado A., Herrero A., 1988, A&A, 207, L5
Milne D. K., Aller L. H., 1975, A&A, 38, 187
Osterbrock D. E., Tran H. D., Veilleux S., 1992, ApJ, 389, 305
Peimbert M., 1967, ApJ, 150, 825
Peimbert N., Storey P. J., Torres Peimbert S., 1993, ApJ, 414, 626 (PSTP)
Pequinot D., Petitjean P., Bonisson C., 1991, A&A, 251, 680 (PPB)
Rudy R. J., Rossano G. S., Erwin P., Puetter R. C., 1991, ApJ, 368, 468
Schonberner B., 1981, A&A, 103, 119
Seaton M. J., 1979, MNRAS, 187, 73P
Smits D. P., 1991, MNRAS, 251, 316
Taylor D., 1990, NASA *IUE* Newsletter, 41, 10
Wiese W. L., Smith M. W., Miles B. M., 1969, Atomic Transition Probabilities, Vol. 2. National Bureau of Standards NSRDS-NBS 22, Washington
Wright W. H., 1918, Publ. Lick Obs., 13, 193
Zuckerman B., Aller L. H., 1986, ApJ, 301, 772